AGU PUBLICATIONS

Earth and Space Science

REVIEW
10.1002/2014EA000051

Key Points:
- Ground-based and satellite-based lightning data are complementary in nature
- Validation is critical to properly utilizing LLS data in applications
- Various validation techniques can be used to evaluate the performance of LLSs

Correspondence to:
A. Nag,
amitabh.nag@vaisala.com

Citation:
Nag, A., M. J. Murphy, W. Schulz, and K. L. Cummins (2015) Lightning locating systems: Insights on characteristics and validation techniques, *Earth and Space Science*, *2*, doi:10.1002/2014EA000051.

Received 28 OCT 2014
Accepted 4 FEB 2015
Accepted article online 13 FEB 2015

Lightning locating systems: Insights on characteristics and validation techniques

Amitabh Nag[1], Martin J. Murphy[1], Wolfgang Schulz[2], and Kenneth L. Cummins[3]

[1]Vaisala Inc., Louisville, Colorado, USA, [2]OVE-ALDIS, Vienna, Austria, [3]Department of Atmospheric Sciences, University of Arizona, Tucson, Arizona, USA

Abstract Ground-based and satellite-based lightning locating systems are the most common ways to detect and geolocate lightning. Depending upon the frequency range of operation, LLSs may report a variety of processes and characteristics associated with lightning flashes including channel formation, leader pulses, cloud-to-ground return strokes, M-components, ICC pulses, cloud lightning pulses, location, duration, peak current, peak radiated power and energy, and full spatial extent of channels. Lightning data from different types of LLSs often provide complementary information about thunderstorms. For all the applications of lightning data, it is critical to understand the information that is provided by various lightning locating systems in order to interpret it correctly and make the best use of it. In this study, we summarize the various methods to geolocate lightning, both ground-based and satellite-based, and discuss the characteristics of lightning data available from various sources. The performance characteristics of lightning locating systems are determined by their ability to geolocate lightning events accurately with high detection efficiency and with low false detections and report various features of lightning correctly. Different methods or a combination of methods may be used to validate the performance characteristics of different types of lightning locating systems. We examine these methods and their applicability in validating the performance characteristics of different LLS types.

1. Introduction

The geolocation of lightning discharges, or particular physical processes within discharges, is important in a wide variety of applications. These include lightning warning and safety applications, thunderstorm nowcasting and forecasting, locating lightning-caused damage to resources and infrastructure, risk assessment, geophysical research, insurance, and a variety of other real-time and forensic applications. Typical users of lightning information include national and regional meteorological agencies and aviation or air traffic authorities including space launch facilities, land management entities, forest services, electric power transmission and distribution operators, wind farm operators, and other public utilities.

The most common way to geolocate lightning is by using a lightning locating system (LLS), which may be a ground-based or satellite-based electromagnetic (including optical) sensor or a network of sensors. A ground-based LLS is typically a network of a minimum of four to five sensors and a central processor. Each sensor measures the electromagnetic signal produced by a lightning discharge and sends back information about the associated waveform characteristics to the central processor. An LLS sensor may operate at frequencies ranging from ELF to UHF. Once a specific lightning event is measured by multiple sensors in a network and reported to the central processor, one or more techniques can be used at the central processor to geolocate the lightning event. Ground-based LLSs have been operating since the 1920's and modern LLSs are able to determine the location, intensity, and type of lightning, and track the movement of thunderstorm cells and the evolution of their charge structure in real time.

Low-Earth orbiting satellite-based LLSs that use a focal plane array for optical measurements in the near infrared [e.g., *Christian et al.*, 1996, 1999] have provided lightning data over large fields of view for more than two decades. Additionally, VHF antenna systems on board low-Earth orbiting satellites [e.g., *Jacobson et al.*, 2011; *Morimoto et al.*, 2011] can be used to detect lightning over large regions. Data from on-board sensors are processed locally to filter out noise and geolocate lightning events. The first geostationary satellite-based LLS is expected to be launched in the near future (March 2016; S. Goodman, personal communication, 2014; see also http://www.goes-r.gov/mission/news.html).

Lightning data from different types of LLSs often provide complementary information about thunderstorms. For example, a good estimate of the fraction of cloud flashes in a thunderstorm may be obtained by combining the information from an LLS that reports cloud-to-ground lightning with high detection efficiency and low misclassification (see section 4) but is not able to detect all cloud lightning flashes in the storm, with information from an LLS that reports nearly all cloud and cloud-to-ground flashes in the storm but is not able to discriminate between flash types [e.g., *Boccippio et al*., 2001b; *Koshak*, 2010; *Medici et al*., 2015]. For all the applications of lightning data, it is critical to understand the information that is provided by various LLSs in order to interpret it correctly and make the best use of it. In this study, we briefly review the characteristics of electromagnetic emissions from lightning processes at various frequency ranges, the propagation paths of these emissions, and how these relate to the design of modern LLSs and the characteristics of data available from them. We then summarize the various methods of lightning geolocation used in ground-based and satellite-based LLSs. Finally, we discuss in detail the performance characteristics of various types of LLSs, and the methods used to validate them. We do not discuss single-point lightning sensors that use electromagnetic waveform parameters to estimate location of lightning events relative to the sensor location.

2. Electromagnetic Emissions From Lightning and Their Impact on LLS Design and Characteristics

Lightning flashes, both cloud and cloud-to-ground, may have durations of a second or more, while individual processes within a particular flash may last from a few hundred milliseconds to a few microseconds or less. These processes produce electromagnetic signatures in the range from a few hertz (long continuing currents) to 10^{20} Hz (hard X-rays) [*Rakov*, 2008]. Gamma ray emissions (terrestrial gamma-ray flashes) have been observed to occur in association with lightning [e.g., *Cummer et al*., 2005, 2011]. The peak radiated power in the radio frequency range from lightning is expected to be at about a few to 10 kHz and to fall off linearly with increasing frequency [e.g., *Serhan et al*., 1980; *Weidman et al*., 1981; *Cummins and Murphy*, 2009, Figure 2]. Due to the wide range of rates and amplitudes of electromagnetic emissions from different lightning processes [*Malan*, 1963], different frequency ranges are best suited for detecting them. Table 1 provides an overview of the characteristics of lightning processes at various frequency ranges commonly detected and geolocated by different LLSs including their typical peak amplitudes normalized to a distance of 100 km, the associated modes of signal propagation, and typical numbers of emissions in each lightning flash. These characteristics of lightning electromagnetic signals determine how LLSs are designed, their effective ranges (or areas of coverage), and the characteristics of the data available from them. For example, ground-based LLSs operating at ELF-VLF-LF ranges are typically referred to as "long-range" LLSs because electromagnetic radiation from lightning is the most powerful in this frequency range and the signals have wavelengths typically in the range of 10–100 km and propagate through the Earth-ionosphere waveguide, such that they can be measured by long-range LLS sensors at distances of a few thousand kilometers from the location of the lightning process. On the other hand, ground-based LLSs operating at VHF are referred to as "short-range" LLSs because electromagnetic radiation from lightning in this frequency range has wavelengths of about 1–10 m and has to be measured by LLS sensors within line-of-sight distance of the lightning process. Emissions in the high radio-frequency range (e.g., VHF) and optical signals can be detected from satellite-based sensors, whose design and operating characteristics are dictated by the field of view and the orbital characteristics of the satellite platform. The net result is that different types of LLSs provide complementary information about thunderstorms and a variety of different techniques are needed to assess or validate the performance characteristics of different LLSs (as discussed in section 5).

3. Lightning Geolocation Techniques

The two most common techniques used for lightning geolocation in ground-based LLSs are time-of-arrival (TOA) and direction finding (DF) [e.g., *Cummins et al*., 1998; *Cummins and Murphy*, 2009; *Rakov*, 2013]. Low-Earth orbiting, satellite-based LLSs use either optical imaging [e.g., *Christian et al*., 1989] or a VHF direction-finding technique [e.g., *Jacobson et al*., 2011; *Morimoto et al*., 2011, 2014] to geolocate lightning.

3.1. Time of Arrival

The time-of-arrival technique uses the occurrence time of a specific feature of the electromagnetic waveform (e.g., onset time, time of peak magnitude, or zero-crossing time) of a lightning event measured

Earth and Space Science

10.1002/2014EA000051

Table 1. Characteristics of the Lightning Processes Commonly Detected and Geolocated by Different LLSs[a]

Frequency Range	Approximate Wavelength Range	Discharge Process(es) / Lightning Event(s)	Typical Spectral Amplitude in dB (V/m/Hz) Normalized to 100 km[b]	Mode of Signal Propagation	Typical Number of Emissions per Flash (Order of Magnitude)	LLS Type / Comments
VLF (3–30 kHz)	10–100 km	CG RS, CIDs	−76 to −86 (10 kHz) for return strokes	Ground wave and Earth-ionosphere waveguide (affected by dispersion due to finite soil conductivity and characteristics of ionosphere)	1–10	Long range, ground based
		Large-amplitude cloud pulses including PB	—		1–100	
LF and MF (30 kHz to 3 MHz)	0.1–10 km	CG RS	−92 to −110 (100 kHz)		1–10	Medium range or short range, ground based, depending on sensor sensitivity and baselines
		Cloud pulses including PB, CIDs, and K-changes	−105 to −125 (100 kHz)		1–100	
		CG leader steps	−116 to −126 (300 kHz)		10	
HF (3–30 MHz)	10–100 m	Various in-cloud and leader processes	−136 to −146 (3 MHz)	"Mixed" ground wave and line of sight (affected by blockage due to presence of objects in line of sight)	10–100	Short range, ground based
VHF (30–300 MHz)	1–10 m	Breakdown of "virgin air" during channel formation	−160 to −190 (rough estimate for frequency ranges from 20–400 MHz)	Line of sight (affected by blockage due to presence of objects in line of sight)	10–1000	Short range, ground based, using TOA
		Dart leaders and K-changes, CIDs			10–100	Short range, ground based using ITF
Near IR / optical (30–300 THz)	10^{-7} to 10^{-6} m	Hot current-carrying channels	NA (different unit of measurement)	Line of sight (affected by scattering in clouds)	10–100 groups per flash	Satellite based

[a]CG RS = cloud-to-ground return stroke; CID = compact intracloud discharge; PB = preliminary breakdown; TOA = time of arrival; ITF = interferometry.
[b]Spectral amplitude data gleaned from *Serhan et al.* [1980], *Weidman et al.* [1981], *Horner* [1964], *Oetzel and Pierce* [1969], *Kosarev et al.* [1970], and *Willett et al.* [1989a, 1989b] and then normalized to a distance of 100 km assuming a 1/distance dependence.

simultaneously at multiple sensors. A constant difference of the times at which a specific feature occurs at two different sensors defines a hyperbola, and multiple sensor pairs provide multiple hyperbolas whose intersections identify a lightning event location. Under some conditions, hyperbolas produced from only three sensors will result in two closely spaced intersections, thus leading to an ambiguous location [e.g., *Cummins and Murphy*, 2009, Figure 3]. Thus, the TOA technique requires simultaneous measurements of a lightning event from at least four sensors in order to geolocate the event uniquely, including calculation of its time, latitude, and longitude. In order to calculate the altitude of a lightning event, simultaneous measurements by at least five sensors are required. The TOA technique can be applied in ground-based LLSs operating in any frequency range. *Lugrin et al*. [2014] describe the electromagnetic time reversal technique that may be used to geolocate lightning, and they mathematically demonstrate TOA to be a particular case of this technique.

In the TOA technique, a fixed random error in the time measurement results in a fixed random error in the calculated position as long as the lightning event occurs within the perimeter of the set of sensors. The position error is thus directly proportional to the timing error and independent of the distance between the sensors and the lightning event. Further, the TOA technique is not affected by directionally dependent local angle errors (known as "site errors"). The primary factors introducing timing error are variations in terrain elevation (introducing delay in the arrival time of lightning electromagnetic signals) and propagation over finite conductivity soil (introducing arrival time delay and frequency dependent attenuation of signals). Factors such as GPS error, nonvertical lightning channels, and complexities of lightning electromagnetic wave shapes also contribute (generally to a lesser extent) to the timing error. Timing error introduced by terrain and soil conductivity variations can be addressed by applying location-specific corrections to the arrival times measured by LLS sensors [e.g., *Cooray*, 1987; *Cummins et al*., 2010; *Honma et al*., 2013].

The lightning electromagnetic waves measured by sensors in long-range LLSs are affected by propagation over thousands of kilometers in the Earth-ionosphere waveguide. As a result, accounting for timing error introduced by terrain, soil conductivity variations, and ionosphere conductivity and height variations is of fundamental importance when using the TOA technique, and in this case, the definition of "time-of-arrival" differs from simply measuring the time of a specific feature on a waveform. For example, the World Wide Lightning Location Network (WWLLN) uses a technique called the time-of-group-arrival (TOGA). This method is based on the fact that lightning VLF signals (sferics) propagating in the Earth-ionosphere waveguide experience dispersion, in that the higher-frequency components arrive earlier than the lower-frequency components [*Dowden et al*., 2002]. The time at which the derivative of phase with respect to frequency reaches zero in any sferic measured by a WWLLN sensor is used as a dispersion-corrected time and yields better results than a simple trigger time. Once this corrected time is determined at multiple sensors, the essential TOA technique is then applied in the usual way to calculate the time, latitude, and longitude of the associated lightning event. In the Global Lightning Dataset (GLD360), TOA is used in combination with direction-finding (see section 3.2) to geolocate lightning. In order to select the most appropriate time feature, a waveform correlation algorithm is used in each sensor [*Said et al*., 2010]. A bank of "canonical" lightning waveforms corresponding to propagation over different distance ranges are used for this purpose. Discussion of the performance characteristics of long-range and medium-range LLSs is found in section 4.1.

3.2. Direction Finding

The direction finding technique typically employs magnetic direction finding (MDF), generally used in the VLF and LF-MF ranges, or interferometry, generally used in the VHF range (even though it has been used recently in the LF range [*Lyu et al*., 2014]).

The magnetic direction finding technique generally uses two orthogonal loop antennas to measure the magnetic field waveform produced by a lightning event. The ratio of the amplitudes of a selected waveform feature (generally the peak) measured by each loop can be used to calculate the azimuth of a lightning event location with respect to a sensor location, which gives a direction vector joining a sensor location and a lightning event location [*Krider et al*., 1976]. The intersections of two or more such direction vectors from two or more sensors measuring the same lightning event simultaneously identify a lightning event location. The time, latitude, and longitude of a lightning event can be calculated using this technique. In order to calculate the altitude of a lightning event, two or more three-axis magnetic field sensors are required, with each sensor having three orthogonal loop antennas and the ability to measure both the azimuth and elevation angles of a lightning event.

In VHF interferometry, each sensor consists of an array of closely spaced antennas, with the separation distance between individual antennas in the array being much smaller than the distance between the array and the lightning event location. The arrival-angle (azimuth) information can be derived from arrival time (phase) difference of the VHF signals associated with lightning events between individual antennas in a sensor. Similar to the MDF technique, simultaneous measurements of the azimuth of a lightning event location at two or more sensors can be used to determine the event location. The time, latitude, and longitude of a lightning event can be calculated using this technique. In order to add altitude to the geolocation, two or more sensors must simultaneously measure the azimuth and elevation angles of the event. VHF interferometry may be performed in narrowband [e.g., *Lojou et al*., 2009] or broadband [e.g., *Shao and Krehbiel*, 1996; *Mardiana and Kawasaki*, 2000; *Sun et al*., 2013; *Stock et al*., 2014].

In ground-based LLSs, both MDF and interferometric techniques have to account for directionally dependent local site errors (typically due to various types of electromagnetic coupling) for each sensor in order to get accurate angle estimates. Given constant angle error, the location error associated with the estimated position of a lightning event is proportional to the distance between the sensors and the lightning event. That is, a constant angle error at the sensor translates to increasing linear error as the distance from the detector to the event increases. Additionally, when only two sensors are used to estimate position, the location error is much larger near the line joining the two sensors than it is where the sensor direction vectors intersect at a right angle.

3.3. Optical Imaging

Optical emissions from cloud-to-ground and intracloud lightning discharges can be detected from above cloud top. The strongest emissions in the cloud-top lightning optical spectra [e.g., *Christian et al*., 1989, Figure 1] are produced by the neutral oxygen (at 777.4 nm wavelength) and neutral nitrogen (at 886.3 nm wavelength) lines in the near infrared. Roughly 5% of the optical energy in a lightning flash may be radiated at and around each of these wavelengths. In satellite-based LLSs, lightning events (or groups of lightning events, see section 4.3) are geolocated by using geometric projection of images taken from space of optical radiation from lightning within clouds. The time, latitude, and longitude of a lightning event (or a group of events) can be calculated using this technique. Altitude of lightning events, however, cannot be determined. Detailed discussion of the factors that must be considered in satellite-based optical imaging can be found in *Boccippio et al*. [2000], *Suszcynsky et al*. [2001], *Boccippio et al*. [2002], *Christian et al*. [2003], and *Mach et al*. [2007].

3.4. Combined and Special Techniques

Long- and medium-range LLSs (see section 4.1) may use a combination of TOA and MDF techniques in order to utilize the combined strengths of both techniques. With direction-finding alone, a minimum of only two sensors can provide a geolocation but the position error is subject to the distance-dependent growth discussed in section 3.2, and it is necessary to correct the site errors affecting the angle measurements. With TOA alone, more sensors are required to determine a geolocation, but position errors are independent of distance inside the network and are generally lower than those produced from direction-finding alone. In combined TOA-MDF LLSs, lightning events may be geolocated by as few as two contributing sensors and benefit from the position error advantage of TOA in the interior of the network, although there are larger location errors near the line joining the two sensors as described in section 3.2.

Broadband VHF interferometry, using a two-antenna system to estimate a direction of arrival, has been used along with optical imaging to geolocate lightning in low-Earth orbiting satellite-based LLSs [*Morimoto et al*., 2014]. *Jacobson et al*. [2011] used a noninterferometric VHF direction-finding technique to geolocate thunderstorms approximately with data from two orthogonal VHF log-periodic antennas on the Fast On-orbit Rapid Recording of Transient Events (FORTE) satellite. This technique does not require combination with optical imaging to perform geolocation but is subject to 180° ambiguity (hence, two possible geolocations per detected pulse). Discussion of the performance characteristics of satellite-based LLSs using VHF direction finding techniques is found in section 4.2.

Medium range LLSs may use a combination of sensors operating in the VLF to MF and VHF ranges [e.g., *Lojou et al*., 2009; *Murphy et al*., 2013]. Since different frequency ranges are suitable for measuring emissions from different types of lightning processes (as discussed in section 2), such medium range LLSs are able to

geolocate lightning processes such as return strokes and cloud pulses using measurements made in the VLF to MF range (discussed in section 4.1) and map the full spatial extent of lightning channels using measurements made in the VHF range (discussed in section 4.2).

4. Performance Characteristics of LLSs Operating at Various Frequency Ranges

The performance characteristics of an LLS refer to its ability to detect, locate, and report various aspects of lightning discharges. These performance characteristics include (1) detection efficiency (DE) for cloud and cloud-to-ground flashes and cloud-to-ground strokes, (2) the associated location accuracy (LA), (3) polarity and peak current estimation accuracy, and (4) lightning type classification accuracy, the ability to differentiate between different processes such as in-cloud pulses and cloud-to-ground strokes. Table 2 summarizes the ranges of validated or estimated performance characteristics that are germane to each type of LLS given the signals measured and the information that can be derived from those signals. The various studies from which the information in Table 2 is derived are discussed in the following subsections. Note that various measurements made by LLSs operating at VHF–UHF ranges (see section 4.2) and visible and near infrared frequency ranges (see section 4.3), such as spatial extent of a lightning flash and peak radiated source power or radiant energy, are not easily verified and, therefore, not included in Table 2. Total lightning detection is the detection and geolocation of events associated with a large fraction of cloud and cloud-to-ground flashes that occur within the coverage area of an LLS. In Table 2 we provide the total flash detection efficiency for ground-based and satellite-based LLSs that detect the majority of cloud and cloud-to-ground flashes but cannot distinguish between them. For satellite-based LLSs, the spatial resolution of their imaging systems is often used as a measure of their location accuracy. Data elements that are not typically provided by a particular LLS type are indicated by "NA," and information that cannot be provided at the discharge process (or event) level but is available at the flash level is indicated.

A fifth LLS performance characteristic (not included in Table 1) is the rate of false detections. Studies on false detections by LLSs are very sparse compared to those related to the validation of the four performance characteristics listed in the previous paragraph. The false detection rate is inherently challenging to quantify and is not subject to any of the validation methods discussed in section 5 which involve the use of independent measurements of lightning to assess the performance of LLSs. Appendix A provides some information about defining false detections and quantifying and evaluating their rate of occurrence for ground-based LLSs. Factors contributing to false detections in satellite-based LLSs and methods to minimize them are mentioned in section 4.3.

4.1. LLSs Operating at ELF to HF

ELF, VLF, LF, MF, and HF radiation is produced by lightning processes ranging from the relatively long-duration continuing currents, which last for several tens to hundreds of milliseconds, to the relatively short-duration currents flowing through cloud and cloud-to-ground lightning channels with total durations of a few to several tens of microseconds. LLSs operating in these frequency ranges generally detect and geolocate electromagnetic pulses radiated by the latter processes, which include return strokes and M-components in cloud-to-ground discharges and preliminary (or initial) breakdown pulses and other relatively high-amplitude pulses radiated by predominantly vertical channels within the cloud.

Propagation of lightning electromagnetic signals over the Earth's surface (ground wave) causes the amplitude of such signals to decay, with higher frequency components being attenuated more quickly with distance. Figure 1 shows the relative amplitude, as a function of frequency, of the vertical electric field or horizontal magnetic field after propagating 100 km over soil having a conductivity of 10 mS/m using the Norton flat Earth model [*Norton*, 1937] relative to what it would be over perfectly conducting ground. Note that soil conductivity in North America, for example, generally varies from about 1 to 30 mS/m, and that Norton's approximation is valid up to about 1 MHz. At a distance of 100 km, signal amplitudes are expected to attenuate by 12 dB per frequency doubling for frequency components above 400 kHz. The combination of ground-wave propagation with relatively minimal attenuation in the VLF-LF and the fact that lightning-radiated power peaks in the VLF-LF range makes this range of frequencies suitable for long- and medium-range ground-based LLSs. On the other hand, the larger propagation losses and lower radiated power from lightning processes at higher frequencies indicate that the HF components of lightning signals are only useful when measured by sensors within several tens of kilometers of the location of a lightning event. As discussed above, long- and

AGU Earth and Space Science

10.1002/2014EA000051

Table 2. Summary of the Performance Characteristics of Different Types of Modern LLS[a]

LLS Type		Sensor Baseline Distance/Optical Imager Field of View	Detection Efficiency			Median Location Accuracy/Spatial Resolution	Temporal Resolution	CG Stroke Peak Current, Polarity Estimation Error	CG Stroke Location and Multiplicity	Lightning Type Classification Accuracy
			CG Stroke	CG Flash	IC Flash					
Ground based	Long range (VLF)	Several thousand kilometers	3–40%	10–70%	Few to less than 10%	2 km to more than 10 km	Ten to several tens of microseconds	25–30%, 1–4%	Available	NA
	Medium range (ELF-HF)	150–400 km	70–90%	85% to greater than 95%	About 50%	About 100 m to less than 1 km	Several tens of nanoseconds	15–20%, negligible	Available	48–96%
	Short range (ELF-HF)	50–75 km	Greater than 90%	Greater than 95%	About 75%[b]	About 100 m to few hundred meters	Several tens of nanoseconds	15–20%, negligible	Available	48–96%
	VHF mapping	10–40 km for TOA, 150 km or less for interferometry		Total flash DE of greater than 95%		Several tens to few hundred meters	10 μs or more for TOA), 100 μs for interferometry	NA	NA	-
Satellite based	Low-Earth orbit optical imaging/mapping	600 × 600 km to 1300 × 1300 km areas for 90 s to a few minutes		Total flash DE of 38% to 88%, depending upon instrument and time of day[b,c]		Ten to a few tens of kilometers	2 ms	NA	NA	NA[d]
	Geostationary optical imaging/mapping	Two optical imagers on board two satellites (east and west) staring continuously at the Americas and nearby oceans		Total flash DE of 85–90%[b]		8–14 km[b]	2 ms	NA	NA	NA[d]

[a]For geostationary satellite-based LLS to be launched in the near future, the performance characteristics indicated are expected ones. NA = not applicable (indicates information that cannot be observed by the given LLS type), CG = cloud-to-ground, IC= intracloud, TOA = time of arrival.
[b]Estimated performance characteristics derived from the characteristics of sensors, associated instruments, and algorithms.
[c]Ranges from 60% for CG flashes to nearly 100% for IC flashes [*Thomas et al.*, 2000]. See text for details.
[d]Estimation of the fraction of cloud-to-ground flashes in thunderstorms may be available [*Koshak*, 2010; *Koshak and Solakiewicz*, 2011]. See text for details.

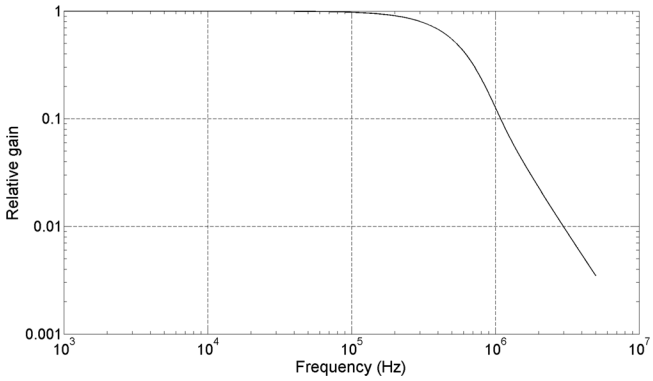

Figure 1. Behavior of vertical electric field or horizontal magnetic field after propagating 100 km over soil having conductivity of 10 mS/m using the Norton flat Earth model which is valid up to about 1 MHz.

medium-range LLSs may use TOA, MDF, or a combination of the two techniques to geolocate lightning. Typically, the performance characteristics of such systems improve as the number of sensors used to cover a particular area is increased, and thus, the distance between adjacent sensors (referred to as the baseline distance) in the network is reduced.

Long-range LLSs, whose adjacent sensors are separated by distances of a few to several thousand kilometers, generally operate in the ELF to VLF range. Such LLSs may provide regional [e.g., *Chronis and Anagnostou*, 2006; *Pessi et al*., 2009; *Morales et al*., 2014] or global [e.g., *Hutchins et al*., 2012a, 2012b; *Said et al*., 2010, 2013] coverage. These systems provide continuous coverage over land and ocean due to their relatively long baseline distances. Lightning data from such systems typically consist of the time of occurrence of each lightning event, latitude, longitude, and a variety of parameters indicating the quality of the geolocation, such as chi-square and confidence ellipse angle and axes lengths. Some long-range LLSs also provide the polarity and estimated peak current (or peak radiated power) of lightning events. At present, long-range LLSs do not distinguish between cloud-to-ground strokes and cloud pulses. However, they are likely to detect primarily cloud-to-ground strokes, with the percentage of cloud lightning pulses detected being very small. This expectation is due simply to the greater amplitudes of the emissions from return strokes in this frequency range.

Performance characteristics of long-range LLSs may vary relatively widely depending upon the characteristics of sensors, geolocation techniques used, and the geographic region being considered. The cloud-to-ground flash DE is in the range of about 10% [e.g., *Mallick et al*., 2014a] to about 70% [e.g., *Mallick et al*., 2014b], the cloud-to-ground stroke DE from about 3% [e.g., *Mallick et al*., 2014a] to 40% [e.g., *Mallick et al*., 2014b], the median LA from about 2 km [e.g., *Mallick et al*., 2014a, 2014b] to over 10 km [e.g., *Chronis and Anagnostou*, 2006; *Morales et al*., 2014], median peak current estimation error of around 25–30% [e.g., *Said et al*., 2013; *Mallick et al*., 2014b], and polarity estimation error of 1–4% [e.g., *Said et al*., 2013; *Mallick et al*., 2014b].

Medium-range LLSs, whose adjacent sensors may be separated by distances as large as 400 km, operate in various parts of the ELF to HF range, even though the majority of the MF-HF component of lightning electromagnetic signals may be lost due to propagation over distances greater than 100 km, as discussed above. Such LLSs may have regional [e.g., *Pinto et al*., 2009; *Shindo et al*., 2012], country-wide [e.g., *Cummins et al*., 1998; *Heckman and Liu*, 2010; *Sugita and Matsui*, 2012], or continental-scale [e.g., *Orville et al*., 2002, 2011; *Schulz et al*., 2014; *Holler et al*., 2012] coverage and are often referred to as precision LLSs as they generally provide precise information about the lightning events geolocated by them. This is, however, applicable only to areas within the perimeter of such medium-range LLSs, which are very often limited to the regional coastlines or boundaries, with performance characteristics gradually falling off outside the boundaries. Data from such systems typically consist of the time of occurrence, latitude, longitude, estimated peak current and polarity, type classification (cloud or cloud-to-ground) of each lightning event, and a variety of parameters indicating the quality of the geolocation such as chi-square and confidence ellipse angle and axes lengths.

The cloud-to-ground flash and stroke DE of modern medium-range LLSs generally range from about 85% to over 95% and from about 70% to over 90%, respectively [e.g., *Nag et al*., 2011a; *Nag and Rakov*, 2014; *Mallick et al*., 2014c, 2014d; *Schulz et al*., 2013, 2014]. The median LA ranges from about 100–200 m [e.g., *Schulz et al*., 2012; *Cramer and Cummins*, 2014; *Mallick et al*., 2014e] to less than 1 km [e.g., *Mallick et al*., 2014d]. The median peak current estimation accuracy is in the 15–20% range [e.g., *Nag et al*., 2011a; *Mallick et al*., 2014c, 2014d], and the polarity estimation accuracy is typically close to 100%.

Modern LLSs operating in the VLF-LF-MF-HF ranges can also detect and geolocate one or more cloud lightning pulses per flash [e.g., *Nag et al*., 2010, 2011b; *Heckman and Liu*, 2010; *Nag et al*., 2014], with the cloud

flash DE being typically about 50% [e.g., *Murphy et al*., 2014; *Cummins et al*., 2014; *Murphy and Nag*, 2015] in medium-range LLSs. In LLSs with baseline distances less than about 150 km, cloud flash DE as high as about 60% has been observed [e.g., *Murphy et al*., 2013], and it is expected to be around 75% in LLSs with baseline distances of 50–75 km. The median location accuracy of cloud pulses (preliminary breakdown pulse trains in cloud-to-ground flashes) was estimated to be 1.5 km by *Murphy et al*. [2014].

For lightning events identified independently as negative cloud-to-ground return strokes, LLSs have classification accuracies ranging from 48% [*Mallick et al*., 2014d] to 96% [*Mallick et al*., 2014c]. Roughly 90% of all cloud-to-ground lightning is expected to be negative [*Rakov and Uman*, 2003]. For independently identified negative and positive cloud lightning pulses, *Zhang et al*. [2015] reported a classification accuracy of 78% and 100%, respectively. The majority of cloud lightning pulses are expected to be positive (produced by cloud discharges occurring between the main negative and upper positive charge regions). For example, roughly two thirds of all cloud lightning pulses reported by the U.S. National Lightning Detection Network (NLDN) are positive [*Nag et al*., 2014].

4.2. LLSs Operating at VHF and UHF

VHF radiation from cloud and cloud-to-ground lightning is thought to be associated with the breakdown of virgin air as a part of the channel formation process and leader processes that occur in pre-existing channels. The first process produces a VHF radiation signature that consists of well-defined bursts of narrow, microsecond-scale pulses. The second process, on the other hand, may be quasi-continuous for a few milliseconds and does not exhibit distinct peaks in the VHF electromagnetic radiation signature. The TOA technique (discussed in section 3.1) measures the time difference between the occurrence of a specific feature in isolated VHF pulses at different sensors, and it is more likely to detect and geolocate sources of VHF radiation from channel formation processes. The same is expected to apply to the UHF TOA measurements performed by *Proctor* [1981] and *Proctor* [1997]. In VHF interferometry (discussed in section 3.2), on the other hand, the phase difference between individual antennas is calculated by integrating over (typically) 100 μs of VHF radiation, and hence, sources of the longer-lasting VHF radiation from continuous leader processes are generally detected and geolocated.

Because VHF signals do not propagate as ground waves, but rather are blocked by terrain and buildings, LLSs operating in the VHF range are generally short range, with adjacent sensors being separated by distances as large as 150 km for interferometry and typically about 10–40 km for TOA. Such LLSs generally provide regional coverage. Because of the high rate of emissions produced per lightning flash (often resulting in multiple emissions per branch) in this frequency range, the data from such systems allow the "mapping" or "imaging" of the full spatial extent of lightning channels, and hence, such LLSs are often referred to as VHF mapping systems. VHF mapping systems [e.g., *Thomas et al*., 2004; *Lojou et al*., 2009] may be used for real time operational applications (such as lightning warning or thunderstorm nowcasting) or for research. Broadband VHF interferometric systems have been developed in Japan [*Akita et al*., 2011], China [*Sun et al*., 2013], and the United States [*Stock et al*., 2014] and deployed in a number of research campaigns. Typically, the data from such LLSs consist of the time of occurrence, latitude, and longitude of each emission source, and of a variety of parameters indicating the quality of the geolocation such as chi-square and confidence ellipse angle and axes lengths. Some VHF systems, particularly the TOA systems, also provide the altitude of each detected emission. Estimated peak current and polarity of lightning events are not reported by VHF mapping systems (unlike LLSs operating at ELF to HF ranges discussed in section 4.1) because no reliable relationship exists between the peak of either narrowband or broadband VHF signals from lightning and peak currents associated with the radiating sources. However, peak radiated source power is reported by VHF TOA systems [*Thomas et al*., 2001]. Due to different sensitivities of such systems to breakdown in positive and negative cloud charge regions, VHF emissions from in-cloud lightning processes geolocated by them can be used to infer the charge structure of a thundercloud. The sources geolocated by such LLSs are generally above the ground surface (mostly within the clouds), and hence, lightning type classification of the individual sources is not applicable. In order to identify flashes that contain cloud-to-ground strokes unambiguously, it is generally necessary to couple data from VHF mapping systems with data from a reference source such as from video cameras or LLSs operating at ELF to HF ranges [e.g., *Zhang et al*., 2015; *Ushio et al*., 2015]. Also, correlated data from an LLS operating at ELF to HF ranges are needed in order to determine the polarity and peak currents of those strokes.

The total (cloud and cloud-to-ground) flash DE of VHF mapping systems is generally expected to be close to 100% because of the large number of VHF emissions produced by each lightning flash coupled with a reasonable probability of detection per emission. DE values approaching 100% in an operational VHF mapping system were found by *Lojou and Cummins* [2006] by comparing with the cloud-to-ground flashes reported in the interior of the NLDN. The LA of individual VHF events reported by TOA mapping systems is of the order of 10 m in the interior of the network, measured by tracking a balloon-borne transmitter [*Thomas et al*., 2004]. Similar measurements of the event-level LA of interferometric mapping systems are not available. However, at the level of overall lightning flashes (obtained by grouping VHF events that appear to be spatially and temporally clustered), observations from overlapping VHF time-of-arrival and interferometric mapping systems show very similar spatial representations of the same lightning flashes [e.g., *Lojou and Cummins*, 2006].

As discussed in section 3, VHF direction finding techniques have been used in low-Earth orbiting satellite-based LLSs. In general, such LLSs geolocate lightning at the storm [*Jacobson et al*., 2011] or cloud level [*Morimoto et al*., 2014]. Data collected over time by such LLSs can be used in climatological studies, but they cannot provide continuous monitoring of individual thunderstorms. *Suszcynsky et al*. [2000] proposed placing VHF receivers on the Global Positioning System (GPS) satellite constellation to form a network of sensors that would detect and geolocate emissions from lightning processes with continuous coverage using the TOA technique. However, that project has not been realized. Instead, the evolution of satellite-based continuous thunderstorm monitoring seems to have moved toward optical imaging of emissions measured from geostationary orbit [*Goodman et al*., 2013] as discussed in section 4.3.

4.3. LLSs Operating at Visible and Near Infrared Frequency Ranges

Lightning processes involve the formation of channels carrying several kiloamperes of electric current with temperatures often greater than 40,000 K. This is accompanied by intense radiation in the optical frequency range with the peak power typically being of the order of 10^9 W [*Christian et al*., 1989]. These optical emissions are a result of dissociation, excitation, and subsequent recombination of various atmospheric constituents as a result of the sudden intense heating, and primarily occur at discrete atomic lines with some continuum at higher frequencies. Satellite-based optical imagers operating in the visible and near infrared frequency ranges measure these optical emissions and geolocate the associated lightning processes by projecting images taken from space onto the Earth's surface. Various satellite programs including the OSO-2 [*Vorpahl et al*., 1970], OSO-5 [*Sparrow and Ney*, 1971], and Defense Meteorological Satellite Program (DMSP) [e.g., *Turman*, 1978; *Turman and Tettelbach*, 1980; *Orville and Henderson*, 1986] used various optical sensors (photodiodes/photometers) to measure lightning. The Night/Day Optical Survey of Lightning (NOSL) [*Vonnegut et al*., 1983] conducted from the space shuttle used a small hand-held instrument package consisting of a 16 mm cine movie camera and solar cell optical pulse detector and recorder. In general, these satellite-based LLSs had poor location accuracy and detection efficiency, of the order of hundreds of kilometers (due to the low spatial resolution of the optical imagers) and less than 2%, respectively.

Three relatively modern satellite-based LLSs on long-term low-Earth orbiting platforms, OV-1, TRMM, and FORTE contain optical imagers (CCD arrays) with fields of view ranging from 600 × 600 km to 1300 × 1300 km. These are called, respectively, the Optical Transient Detector (OTD), Lightning Imaging Sensor (LIS), and the Lightning Location System. Note that in the FORTE satellite the CCD array and a photodiode detector together comprise the Optical Lightning System (OLS). The OTD, LIS, and OLS CCD arrays are similar but use different on-board processing algorithms. The optical imagers measure the signals emitted at 777.4 nm wavelength, associated with dissociation of molecular oxygen into atomic oxygen due to intense heating produced by lightning processes. Data from such LLSs typically consist of the time of occurrence of each lightning event, latitude, longitude, and radiant energy for each pixel. From OTD and LIS data, flashes are assembled from spatially clustered "groups" of pixels illuminated by optical pulses (referred to as "events") for each 2 ms period, as described by *Mach et al*. [2007]. For the OLS, a grouping method based on coincident observations from the photodiode detector and CCD array is used [*Suszcynsky et al*., 2001]. To date, the radiant energy for each pixel has not been fully utilized because interpretation of this measurement is complicated by variations in the optical properties of the path between the emission and the measurement point. While the radiant energy measured from space is probably a good indicator of radiant energy of the associated lightning processes, it is a 1.9 ms time-integrated value and, therefore, not particularly useful

for estimating peak currents of individual lightning events. Also, since photons are neutral particles, optical measurements provide no information on polarity of lightning events. Hence, estimated peak current and polarity of lightning events are not reported by satellite-based LLSs (unlike LLSs operating at ELF to HF ranges discussed in section 4.1).

Performance characteristic estimates of satellite-based LLSs can be derived from the characteristics of their optical sensors and associated instruments. For CCD array-based optical imagers, the absolute location accuracy for lightning events or groups of events depends upon the equivalent pixel size of the detector array, the focal length of the lens, the orbital altitude (which determines the spatial resolution), the effect of scattering of light within the cloud, and the quality of the satellite navigation. The spatial resolution at nadir of the optical images on board the OV-1 and FORTE was about 8 km with the resolution being poorer toward the edges of the field of view. The lower orbital altitude of TRMM resulted in a 4.5 km spatial resolution. The detection efficiency is determined by the final signal-to-noise ratio for each detector element, which is determined by the strength of the lightning optical signal, pixel integration time, the pixel spatial resolution, background illumination (time-of-day), and external noise sources. This signal-to-noise ratio is maximized using high throughput optics (low *f*-number), narrow band filters (1 nm wide), small individual pixel field of view (about 8 km), and low noise electronics. The estimated total flash detection efficiency for LIS during the day and night is estimated to be about 70% and 88%, respectively, and about 38% and 52%, respectively, for OTD [e.g., *Boccippio et al*., 2002; *Cecil et al*., 2014]. False detections, which are a result of intrinsic CCD or sensor hardware noise, optical shot noise, nonlightning optical sources, and high energy particles in the low-Earth orbit spacecraft environment (e.g., the South Atlantic Anomaly) [*Christian et al*., 2003], are removed through variable thresholding techniques and post-processing filtering and the rate of false detection is expected to be insignificant [*Boccippio et al*., 2000]. *Suszcynsky et al*. [2001] describe a technique that uses coincident observations from the FORTE-satellite-based photodiode detector and CCD array to eliminate false detections.

Some studies [e.g., *Boccippio et al*., 2000; *Thomas et al*., 2000; *Kirkland et al*., 2001] have examined the performance characteristics of satellite-based LLSs with respect to ground-based LLSs. Using NLDN cloud-to-ground flash data as reference, *Boccippio et al*. [2000] reported the location accuracy of the OTD (on the OV-1 satellite) to be typically between 20 and 40 km with the median being 50 km. The relatively large location errors were attributed to the uncertainty introduced by OTD's pixel resolution (8–24 km) and imperfect satellite navigation (the OV-1 used gravity gradient stabilization which resulted in poor pointing accuracy). OTD's temporal accuracy, defined as the time difference between the occurrence time of the first NLDN-reported return stroke in a flash and that of the brightest optical pulse group reported by the OTD within 2 s and 200 km of the NLDN-reported first stroke, was generally found to be better than 100 ms. The cloud-to-ground flash DE of OTD was estimated to be in the 46–69% range. *Thomas et al*. [2000] examined the total flash DE of the LIS using VHF mapping data from LMA as reference and found that the LIS detected 33% (9 out of 27) of flashes with sources confined to altitudes below 7 km and 99% (99 out of 101) of flashes with sources at altitudes above 7 km. Almost all cloud flashes and 60% of cloud-to-ground flashes were detected by the LIS. Using the location of a ground-based laser as reference, *Suszcynsky et al*. [2001] estimated the location accuracy of the CCD array-based imager on board the FORTE satellite to be in the range of 5 to 15 km. *Kirkland et al*. [2001] reported the cloud-to-ground flash detection efficiency of the silicon photodiode detector on board the FORTE satellite to be 23% using NLDN data as reference.

While satellite-based LLSs detect optical emissions from both cloud and cloud-to-ground flashes, they cannot distinguish between emissions associated with different lightning types, at least for individual flashes [*Goodman et al*., 1988]. *Koshak* [2010] examined seven optical characteristics of flashes (radiance, area, duration, number of events, and number of groups) and groups (maximum number of events in a group and maximum group area) using data from the OTD (and associated NLDN data) and reported that these characteristics were similar for cloud and cloud-to-ground flashes. However, since the overall mean, median, and standard deviation values of these characteristics for populations of cloud flashes were different from those for populations of cloud-to-ground flashes, the fraction of each lightning type in storms could be estimated. *Koshak and Solakiewicz* [2011] introduced a statistical technique to estimate the fraction of cloud-to-ground flashes in thunderstorms observed by satellite-based LLSs like OTD and LIS. Note that similar to VHF lightning mapping systems, optical imagers are able to map the spatial extent of flashes, although with poorer temporal and spatial resolution, and hence may be viewed as lightning mapping systems. Since

Table 3. Performance Characteristics of Different Types of LLSs That Can Be Validated Using the Different Techniques Discussed in Section 5[a]

	LLS Type			
Validation Technique	Long Range (ELF-VLF)	Medium Range (ELF-HF)	VHF Mapping	Visible and Near Infrared (Satellite Based)
LLS self-reference	Estimated DE (CG stroke, CG flash), estimated LA	Estimated DE (CG stroke, CG flash, IC flash), estimated LA (CG strokes and IC pulses)	Estimated DE (IC flash)	NA
Rocket-triggered lightning and lightning strikes to tall objects	DE (CG stroke), DE (CG flash), LA (CG stroke), polarity and peak current estimation accuracy	DE (CG stroke), DE (CG flash), LA (CG stroke), polarity and peak current estimation accuracy, lightning type classification accuracy	DE (CG flash) approximate LA (CG flash)	DE (CG flash), DE (CG stroke), approximate LA (CG flash)
Video camera measurements	DE (CG stroke), DE (CG flash), DE (IC flash), relative LA (CG subsequent stroke), polarity estimation accuracy (with electric field data)	DE (CG stroke), DE (CG flash), DE (IC flash), relative LA (CG subsequent stroke), polarity estimation accuracy (with electric field data)	DE (CG flash), DE (IC flash)	DE (CG flash), DE (CG stroke), DE (IC flash),
Intercomparison among LLSs	see Table 4	see Table 4	see Table 4	see Table 4

[a]CG = cloud-to-ground, IC = intracloud, NA = not applicable.

these optical imagers on low-Earth orbiting satellites observe a given location on Earth's surface for a limited time (90 s to a few minutes), they can only take snapshots of thunderstorms and cannot monitor them as they develop and evolve. Because of the short viewing times, the detection efficiency values given above are not equivalent to the detection efficiencies of LLSs that geolocate lightning continuously on global or regional scales. Rather, they are conditional probabilities of detection subject to the short viewing time of any given thunderstorm. However, since the detection efficiencies of such optical detectors generally remain constant over space and time, properly computed global lightning climatologies obtained using such data sets are spatially consistent.

The first geostationary satellite-based LLS called the Geostationary Lightning Mapper (GLM) is expected to be launched in the near future (March 2016) on board the GOES-R satellite series. It will have a full-disk (hemispheric) field of view and continuous coverage in time [*Goodman et al*., 2013]. A combination of two such optical imagers on board two geostationary satellites (GOES-E over 75 W longitude and GOES-W over 137 W longitude) is expected to provide continuous coverage (with some overlap) over a region extending from about southern Canada in the north to southern tip of South America in the south and from about the west coast of Africa in the east to eastern New Zealand in the west. The GLM is a near-infrared optical event detector (centered at 777.4 nm wavelength as with LIS/OTD) with a time resolution of 2 ms and a spatial resolution of 8 km at the equator, expanding to 14 km at the edges of the field of view. The GLM will detect both cloud and cloud-to-ground flashes. However, as discussed above, it is not expected to be able to classify individual flashes. The total flash DE is expected to be about 80%, on average, with it being as high as 100% at night. Launch of a geostationary satellite-based LLS with coverage over Europe and Africa is also being planned by the European Space Agency [*Finke et al*., 2010; *Grandell et al*., 2010].

5. Evaluation/Validation of Lightning Locating System Performance Characteristics

The performance characteristics of an LLS determine the quality of the lightning data available. The cloud and cloud-to-ground flash DE, cloud-to-ground stroke DE, LA, polarity and peak current estimation accuracy, and lightning type classification accuracy for various LLSs are discussed in section 4 and summarized in Table 2. In this section, we now discuss the various methods by which these performance characteristics can be evaluated and/or validated. It is generally not possible to validate all LLS performance characteristics using any one method reviewed here. In Table 3, we summarize the various performance characteristics that can be validated using each of these methods. Often, a combination of one or more of the validation techniques discussed in sections 5.1 to 5.4 along with supplementary measurements are used to validate the performance of LLSs. Examples of such studies include *Schulz et al*. [2012], *Cummins et al*. [2014], *Mallick et al*. [2014c], *Poelman et al*. [2013a], and *Zhang et al*. [2015].

5.1. LLS Self-Reference

In this technique, statistical analysis of parameters reported by LLSs [e.g., *Schulz*, 1997] such as standard deviation of sensor timing error, semimajor axis length of the 50% confidence ellipse, and the number of sensors reporting (NSR), is used to infer the LA and DE of an LLS. Examples of studies using this method include *Cummins et al*. [2010], *CIGRE* [2009], and *Honma et al*. [2013]. Parameters suitable for such analysis are currently available from ground-based LLSs only, and hence, this method only applies to such systems. This method requires data collected by an LLS after it has been properly calibrated. It can provide a good estimate of an LLS' performance in a cost-effective, practical manner. It does not, however, provide any absolute measure of either DE or LA, and polarity and peak current estimation accuracy and lightning type classification accuracy of an LLS cannot be evaluated using this method.

While the primary focus of this section is the validation of LLS performance, it is also important to note that LLS performance can be modeled, and LLS self-reference methods of validation are often coupled with performance modeling. For this reason, we review methods of LLS performance modeling in Appendix B. With regard to DE, there is a theoretical relationship between the probability of detection of a cloud or cloud-to-ground event (the event detection efficiency) and the number of sensors that detect (or "report") these events in an LLS. The DE is not directly observable by the LLS, but the distribution of the NSR is. An LLS performance model can be used to calculate both DE and the expected distribution of the NSR, and then, in the self-reference validation step, the observed NSR distribution is compared with the modeled NSR distribution. The relationship between the NSR distribution and the event DE depends upon a variety of factors that are discussed in detail in Appendix B. As an example, in Figure 2a, we show the expected (or modeled) cloud-to-ground stroke DE of an LLS, and in Figure 2b, we show the distributions of the NSR expected at positions A, B, C, and D shown in Figure 2a, for strokes with peak current of 20 kA. By comparing modeled and observed distributions of NSR, it is possible to ascertain whether the actual stroke DE of the LLS is similar to the expected stroke DE (such as the one shown in Figure 2a). In general, the distribution of NSR tends toward lower values as DE decreases with increasing distance from the interior of the network (as we move from point A to D). However, note that, the absolute minimum NSR required to geolocate a stroke, two in this example network, never becomes the most probable value of NSR. This is due to the relationship between LA and DE in the exterior of a network as discussed in Appendix B.

To determine the expected flash DE of an LLS from an expected event DE, it is necessary to know the average number of events per flash. For cloud-to-ground flashes, this is known as the average flash multiplicity, or number of strokes per flash. A relationship between stroke and flash DE is described by *Rubinstein* [1995] using a distribution of the number of strokes per flash reported by *Thomson et al*. [1984] for Florida. Flash multiplicity may vary regionally and seasonally. *Schulz and Cummins* [2008] provide a relationship between stroke and flash DE based on the average flash multiplicity obtained from LLS data and the actual average flash multiplicity.

The confidence (or error) ellipse represents the spatial distribution of random position errors of an LLS. The confidence ellipse is obtained by cutting the two-dimensional (latitude, longitude) probability distribution of random position errors, which is assumed to be Gaussian, at a particular probability level. Typically, a probability level of 0.5 is chosen, such that the ellipse then represents the median random position error. The ellipse can be calculated for each lightning event, and its size and shape depend on the random errors (specifically the standard deviations) in the measurements from the contributing sensors and the location of the event relative to those contributing sensors. In an LLS operating in the VLF to LF and using a combination of the TOA and MDF methods described in sections 3.1 and 3.2, the random errors in both angle and time measurements are needed to determine the ellipse. Details of the confidence ellipse calculation can be found, e.g., in *Schulz* [1997] and *Cummins et al*. [1998]. The ellipse is only a true measure of random position error if the systematic or bias errors in angle and time (e.g., site-specific angle errors and propagation-related timing errors) have been corrected and the random errors have been described correctly. This is the case once the site error corrections, systematic time error corrections, and expected time and angle standard deviations are applied. Figure 3 shows, as an example, the distribution of the semimajor axis (SMA) length of the 50% confidence ellipse, which is expected to be the median location error, in the interior of the NLDN which is comprised of sensors with root mean square timing errors of 0.4 μs. The SMA length of the 50% confidence ellipse reported by LLSs can be averaged over regions and displayed on maps. Figure 4 shows, for

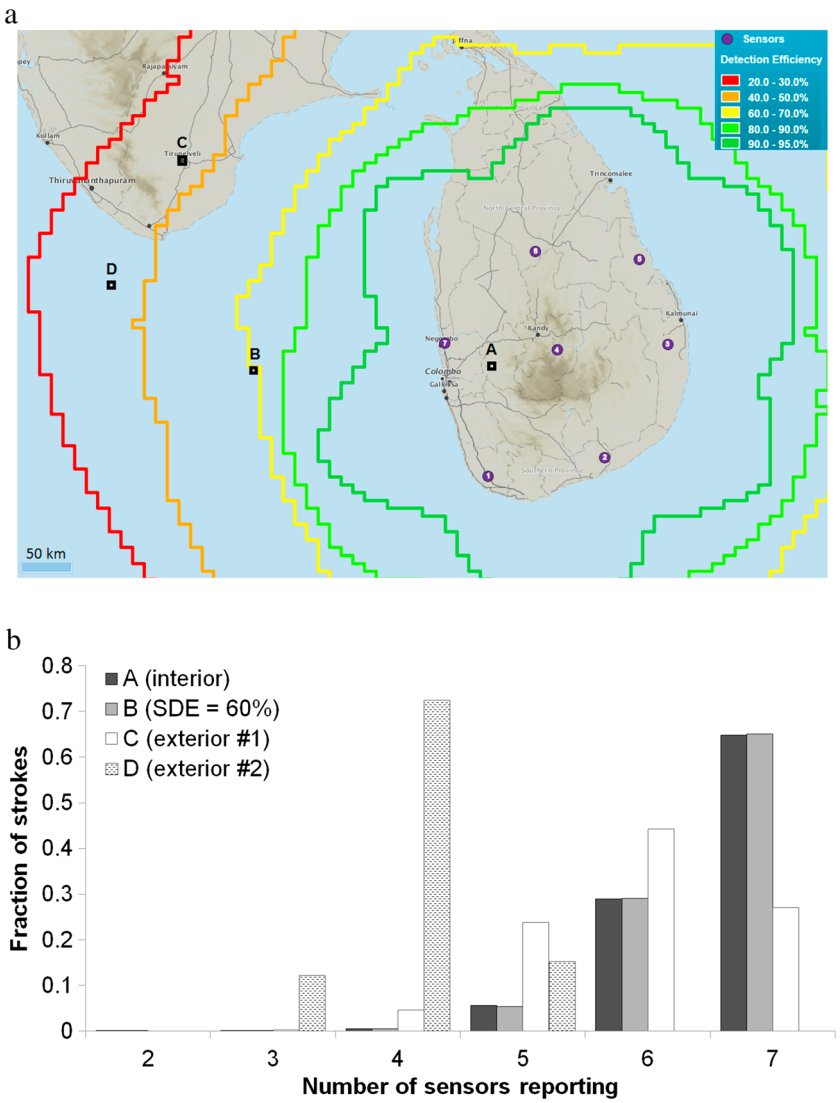

Figure 2. (a) Model estimate of the cloud-to-ground stroke detection efficiency (SDE) of a hypothetical seven-sensor network with sensor locations indicated by circles with numbered labels. The points labeled A, B, C, and D (indicated by squares) are those for which the distributions of the number of sensors reporting (NSR) are shown in Figure 2b. (b) Modeled distributions of the NSR at points A (interior), B (SDE = 60%), C (exterior #1), and D (exterior #2) shown in Figure 2a.

example, the median SMA length of the 50% confidence ellipse for cloud-to-ground strokes in a 50 × 50 km regions for the European EUCLID network in 2013.

5.2. Rocket-Triggered Lightning and Lightning Strikes to Tall Objects

This method uses data from rocket-triggered lightning experiments or lightning strikes to tall objects (e.g., towers instrumented with current measurements) as ground truth to evaluate the performance characteristics of an LLS within whose coverage area the triggered lightning facility or the tall object is located. Since the location of the cloud-to-ground events (including return strokes, M components, and superimposed pulses) and the peak currents are independently known, it is possible to measure the DE, LA, polarity and peak current estimation accuracy, and lightning type classification accuracy of an LLS. Examples of studies using rocket-triggered lightning for LLS performance evaluation include *Jerauld et al.* [2005], *Nag et al.* [2011a], *Chen et al.* [2012], and *Mallick et al.* [2014a, 2014b, 2014c, 2014d]. Examples of studies using lightning strikes to tall objects are found in *Diendorfer et al.* [2000a, 2000b], *Pavanello et al.* [2009], *Romero et al.* [2011], *Schulz et al.* [2012], *Schulz et al.* [2013], and *Cramer and Cummins* [2014]. Data obtained from

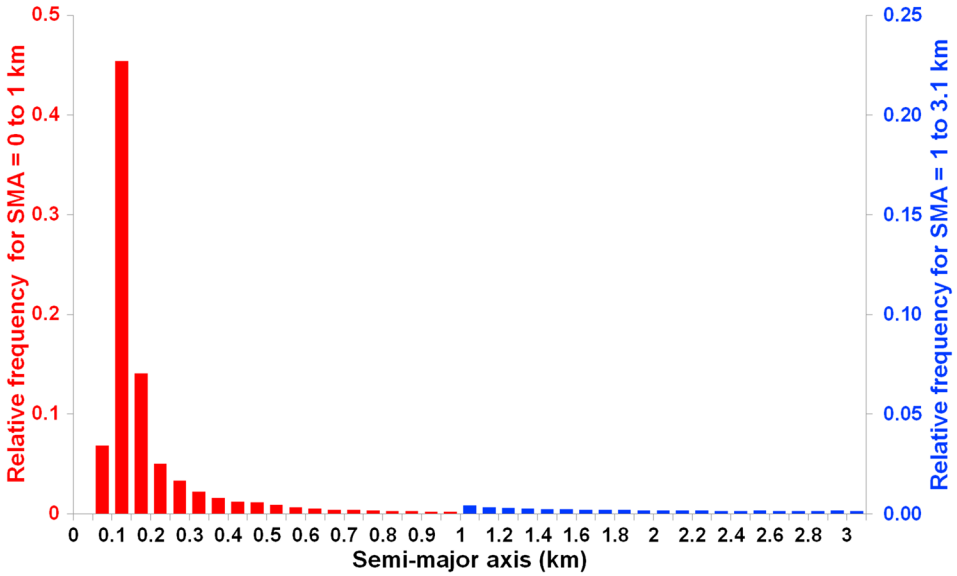

Figure 3. Histogram showing the semimajor axis (SMA) lengths of the 50% error ellipses in approximately 255,000 cloud-to-ground strokes reported within the interior of the U.S. National Lightning Detection Network on 1 day in July 2014. For SMA lengths between 0 and 1 km (red bars), the horizontal axis is in 50 m bins and the vertical axis is shown on the left in red. For SMA lengths between 1 and 3.1 km (blue bars), the horizontal axis is in 100 m bins and the vertical axis is shown on the right in blue.

rocket-triggered lightning and lightning strikes to tall objects can be used to validate the performance characteristics of all ground-based LLSs operating at different frequency ranges and satellite-based LLSs. However, since lightning mapping systems such as LLSs operating at VHF-UHF and satellite-based LLSs do not typically identify ground attachment points, do not estimate polarity or peak currents, and do not provide lightning type classification (see sections 4.2, 4.3, and footnote b of Table 4 for further discussion), only the DE of such LLSs may be validated using this technique. Also, only the cloud-to-ground event and flash DE of an

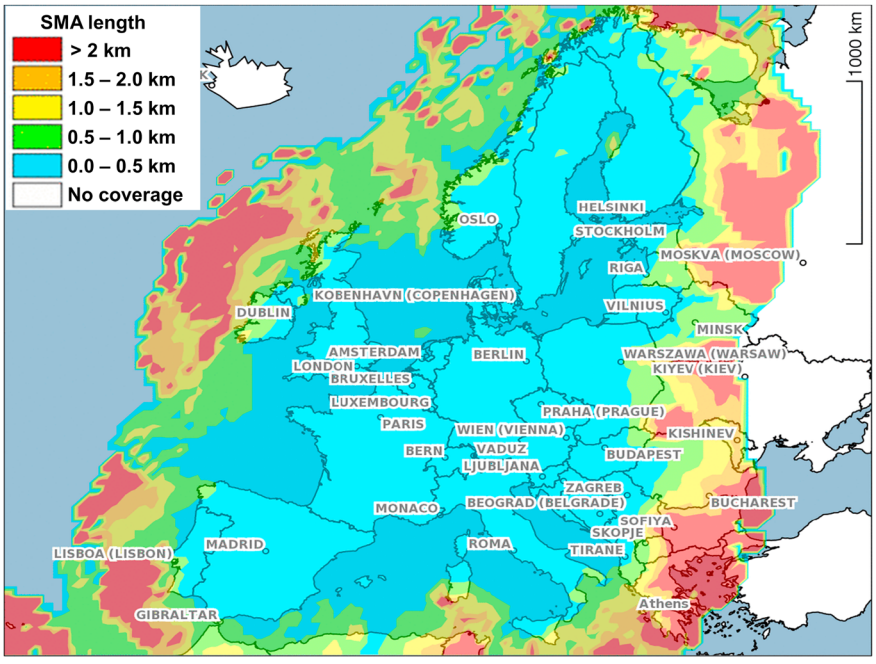

Figure 4. Median of the semimajor axis (SMA) lengths of the 50% confidence ellipse for cloud-to-ground lightning strokes in 50 × 50 km regions for the European EUCLID network in 2013.

LLS operating at ELF to HF can be estimated using these methods as all ground-truth data obtained using these methods are for lightning processes that attach to ground.

Rocket-triggered lightning and lightning strikes to tall objects provide the best ground-truth data for performance characteristics validation for cloud-to-ground lightning and are the only direct ways to validate peak current estimation accuracy of LLSs. However, these studies may be very expensive and may not be practical for all regions (as there are only a few triggered lightning facilities and instrumented towers across the world). Moreover, these are valid indicators of LLS performance only for the region where the rocket-triggered lightning facility or tall object is located, especially in cases where the performance of the LLS is expected to vary significantly from region to region. In order to evaluate the cloud-to-ground stroke LA of an LLS with a large coverage area, multiple noninstrumented tall objects in different regions of the area covered by the LLS may be used [e.g., *Cramer and Cummins*, 2014]. Note that since only 10% of all downward cloud-to-ground lightning is positive, almost all lightning data obtained using rocket-triggered lightning and strikes to tall objects are for negative lightning. Also, upward-initiated lightning from tall towers are often followed by downward negative strokes [e.g., *Diendorfer*, 2010; *Warner et al*., 2012]. LLS performance characteristics inferred using these methods are, therefore, applicable to negative cloud-to-ground lightning only.

The primary distinction between natural cloud-to-ground lightning and classical rocket-triggered lightning is that the stepped-leader/first-return-stroke sequence in natural lightning is replaced by the initial stage (the upward positive leader, involving destruction of the triggering wire, and initial continuous current) in classical triggered lightning. As a result, rocket-triggered lightning provides data for return strokes similar only to subsequent strokes in natural lightning and no data for strokes similar to first strokes in natural lightning can be obtained. *Mallick et al*. [2014c] reported a median peak current of 11.7 kA for 290 triggered lightning strokes; the maximum was 38.1 kA, and the minimum was 2.0 kA. According to *Berger et al*. [1975], the median values of peak current for first and subsequent strokes in natural negative lightning are 30 kA and 12 kA, respectively. The phenomenology of the initial stage of classical triggered lightning is similar to that of upward lightning initiated by tall grounded objects [*Rakov and Uman*, 2003, Chap. 6]. A log-normal relationship is expected between the percentage of upward lightning and effective height (which depends upon the height of the object, local terrain, and other factors) of tall objects [*Eriksson and Meal*, 1984]. Strikes to objects with heights less than 100 m or so are expected to be downward, while objects with heights above 500 m height are expected to experience upward flashes only. Thus, depending upon the height of the object being used for obtaining data for LLS validation, no data for first strokes may be available. Since first strokes in natural lightning are expected to have, on average, peak fields and currents that are a factor of two larger than those for subsequent strokes [e.g., *Nag et al*., 2008], cloud-to-ground flash and stroke DE obtained by rocket-triggered and tall object studies may be somewhat of an underestimate.

When lightning strikes a tall metallic object, the lower part of the lightning channel to ground is replaced by a single grounded vertical metallic conductor through which the return stroke current flows. As a result the characteristics of radiation field waveforms of lightning strokes attaching to tall objects can be quite different than those of radiation field waveforms for strokes attaching to ground [e.g., *Pavanello et al*., 2007a, 2007b; *Pichler et al*., 2010]. This factor needs to be taken into account while using data from lightning strikes to tall objects as ground-truth to examine the lightning type classification of LLSs. Additionally, since in this case the radiator for the lowest several hundred meters (depending upon the height of the tower) is a vertical metallic object instead of an often tortuous and branched natural lightning channel, the return stroke radiation field waveform measured by LLS sensors is expected to have unambiguous rising portions which may be much more suitable for measuring parameters used for lightning geolocation with very small error. As a result, the LA of an LLS estimated using lightning strikes to towers as ground-truth is expected to be somewhat better than that for natural lightning. Finally, since the radiated field peak is influenced by the height of the tower [e.g., *Pavanello et al*., 2007a, 2007b; *Bermudez et al*., 2007], the peak current estimation accuracy of an LLS should be examined using data from lightning strikes to relatively short (less than 150 m or so) towers.

5.3. Video Camera Measurements

Measurements of cloud and cloud-to-ground lightning processes using video cameras can be used as ground-truth to evaluate the performance characteristics of an LLS. The LA, DE, and lightning type classification

accuracy of an LLS can be estimated using this method. Examples of studies using this method include *Idone et al*. [1998a, 1998b], *Ballarotti et al*. [2006], *Biagi et al*. [2007], *Chen et al*. [2012], *Schulz et al*. [2012], *Poelman et al*. [2013a], *Schulz et al*. [2013], *Schulz et al*. [2014], and *Mata et al*. [2014]. Lightning data obtained using video cameras can be used to evaluate the performance characteristics of all ground-based LLSs operating at different frequency ranges and satellite-based LLSs. The advantage of this method is that relatively large sample sizes of ground-truth lightning data obtained at different regions within the coverage area of an LLS can be obtained, rather than at a specific point within network, as is the case for rocket triggered lightning and also typically for lightning strikes to instrumented towers. Note that lightning strikes to multiple (noninstrumented) towers located in different regions within the coverage area of an LLS have been used to evaluate the LA of an LLS, as mentioned in section 5.2. Polarity and peak current estimation accuracy of an LLS, however, cannot be evaluated using data obtained by video cameras alone. A practical problem of performing video camera measurements of lightning flashes is that since the locations of lightning discharges are not known in advance, it may not be easy to capture them in the field of view of the camera. Additionally, sometimes lightning discharges occurring within the field of view of the camera may be obscured by the presence of heavy precipitation or by clouds (in case of cloud lightning).

The absolute LA for cloud-to-ground events (M-components and return strokes) of an LLS operating at ELF to HF can be evaluated using video camera measurements only if two or more correlated video measurements are used to triangulate the location of the lightning channel to ground. The location uncertainty in the camera system employed by *Idone et al*. [1998a, 1998b] was estimated to be as good as about 500 m. However, modern LLSs have expected median location accuracy on the order of a few hundred meters (as discussed in section 4.1). Thus, it is currently impractical for camera-based triangulation to be used to validate absolute LA. Using a single video camera, absolute LA can only be evaluated if the lightning channel attaches to an identifiable ground-based object in the field of view of the camera [e.g., *Mata et al*., 2014]. Otherwise, it is possible to determine the relative LA of cloud-to-ground events in the same channel as the previous stroke in a flash [e.g., *Biagi et al*., 2007]. However, the ground strike points of flashes and channel branching close to ground are often not observed due to obstruction of the video camera's view by closer objects, terrain, and vegetation. Hence, the relative LA determined using this technique may be poorer than the actual LA of an LLS. In order to precisely determine the stroke DE, in addition to the cloud-to-ground flash DE, a high-speed video camera with frame rate faster than the shortest interstroke interval (generally of the order of few to several milliseconds) in cloud-to-ground flashes is needed. The LA of cloud flashes generally cannot be determined by single or multiple correlated video camera measurements because cloud discharges may extend for several tens of kilometers with horizontal branches in several directions and it is likely that significant portions of the channels are either obscured by the presence of clouds or are outside the field of view of the camera. Cloud flash DE and lightning type classification accuracy of an LLS can be determined using this technique only when the complete flash is within the field of view. Video camera measurements are often accompanied by correlated electric or magnetic field measurements. In that case, the DE, LA, lightning type classification accuracy, and polarity estimation accuracy of an LLS can be evaluated, and some ambiguous video measurements may become useable. For example, in order to obtain a reliable cloud-to-ground stroke DE estimate, it is essential to identify M-components and strokes occurring at intervals less than the frame rate of the video camera, and correlated electric or magnetic field measurements can be used for that purpose. Note that polarity is most easily determined if the correlated broadband electric field (rather than magnetic field) is measured.

The LA of VHF mapping systems cannot be determined using video camera measurements, even when multiple correlated video camera measurements are used, as the accuracy of triangulated locations obtained using video cameras is expected to be worse than that of well-calibrated modern VHF mapping systems.

In order to validate the performance of future satellite-based LLSs, ground-based and airborne optical lightning detectors to be used as reference are currently under development (H. Christian, personal communication, 2014). The ground-based optical sensors will be part of a network that includes electric field measuring systems. The airborne optical sensors will consist of an array of optical photometers mounted on high altitude aircrafts such as the NASA ER-2 and the Global Hawk. These photometers will provide high time resolution and low spatial resolution imaging of lightning activity as viewed from above cloud top. In addition to the optical sensors, the ER-2 will fly electric field measuring systems and gamma ray detectors.

Table 4. Lightning Locating System Performance Metrics That Can Be Validated by Intercomparison Among LLSs for Different Types of Test and Reference LLSs[a]

Test LLS Type	Reference LLS Type		
	Long and medium range (ELF-HF)	VHF mapping	Visible and near infrared (satellite based)
Long and medium range (ELF-HF)	DE (CG stroke and flash), LA (CG stroke), polarity and peak current estimation accuracy, lightning type classification accuracy	DE (total flash)[b], approximate LA (IC pulse)	DE (total flash)
VHF mapping	DE (CG flash), approximate LA (CG flash)	DE (total flash), flash spatial extent/ spatial mapping consistency	DE (total flash)
Visible and near infrared (satellite based)	DE (CG flash), approximate LA (CG flash)	DE (total flash), flash spatial extent/ spatial mapping consistency	DE (total flash), flash spatial extent/ spatial mapping consistency

[a]CG = cloud-to-ground, IC = intracloud.
[b]Sometimes a channel to ground is unambiguously seen in three-dimensional VHF mapping data, in which case it may be possible to determine the CG flash DE of a test LLS operating in the ELF-HF range using the VHF data as a reference.

5.4. Intercomparison Among LLSs

The performance of one LLS that is being tested can be compared against another LLS that may be used as reference, as long as the reference LLS is well calibrated, its performance has been characterized independently, and the test and reference networks overlap substantially. This method allows inferences to be made about the DE, LA, polarity and peak current estimation accuracy, and lightning-type classification accuracy of the test LLS relative to the reference LLS. Examples of studies involving different types of test and reference networks include *Lojou and Cummins* [2006], *Said et al.* [2010], *Pohjola and Makela* [2013], *Poelman et al.* [2013b], and *Murphy et al.* [2014]. A mathematical analysis of DE based on LLS intercomparison is provided by *Rubinstein and Montandon* [1992]. LLS intercomparison can be used to evaluate the performance characteristics of all ground-based LLSs operating at different frequency ranges and satellite-based LLSs. The major advantage of the LLS intercomparison technique is that it can use lightning data sets with much larger sample sizes than the techniques discussed in sections 5.2 and 5.3, and they may cover large geographic areas depending upon the coverage areas of the test and reference LLSs. The primary disadvantage, however, is that unlike the techniques discussed in sections 5.2 and 5.3, LLS intercomparisons provide no absolute estimates (based on ground-truth data) of any of the performance characteristics of an LLS.

The exact nature of what can be validated by LLS intercomparison depends on the types of the test and reference networks. Table 4 summarizes the information that can be derived from intercomparisons between LLSs operating at ELF to HF, VHF, and optical and near-infrared ranges. The primary reason for the distinction is that LLSs operating at VHF and those operating at optical and near-infrared ranges are capable of mapping lightning discharges but not capable of differentiating between cloud-to-ground and cloud flashes or of determining polarity or peak current, whereas LLSs operating at ELF to HF have little or no lightning mapping capability but do provide both polarity and peak current estimates, as discussed in section 4. If the reference LLS operates at ELF to HF range, the cloud-to-ground flash and stroke DE, polarity and peak current estimation accuracy, and lightning type classification accuracy of a test LLS operating at ELF to HF range can be estimated with respect the reference LLS. If the test LLS is a VHF or satellite-based mapping system, its DE and LA can be estimated with respect to the reference LLS. If the reference LLS is a VHF or satellite-based lightning mapping system, inference about the total flash DE of a ground- or satellite-based test LLS can be made. Indeed, given that cloud lightning channels are mostly or entirely obscured from direct view of ground-based video cameras and satellite-based optical imagers and the relatively low temporal and spatial resolution of satellite-based LLS data, high-resolution VHF lightning mapping is the only method of doing detailed validation of the cloud lightning DE and LA of another LLS with large sample size lightning data sets. However, as discussed in section 4.3, video cameras have been employed to validate cloud flash DE of LLSs [e.g., *Schulz et al.*, 2012; *Cummins et al.*, 2014] for relatively small numbers (a few hundred or so) of flashes. Note that validation studies using VHF lightning mapping systems as the reference are easily confounded by high flash-rate storms. This is because the source-to-flash grouping algorithms used with VHF mapping data have high uncertainty in situations of high flash rate [*Murphy*, 2006]. While grouping of VHF sources into flashes can be done manually without the use of source-to-flash grouping algorithms, such an analysis can be highly subjective and very time consuming

even for a relatively small number of flashes. Thus, proper validation of cloud lightning DE and LA using VHF mapping systems should be done using only modest flash-rate storms that are fairly isolated from other storms.

Ideally, the performance of the VHF lightning mapping systems should be validated independently. This has been done for the location accuracy of the VHF time-of-arrival LMA system [e.g., *Thomas et al*., 2004]. A balloon-borne VHF transmitter, whose position was measured by GPS, was tracked by an LMA in order to verify the accuracy of the LMA source locations. Interestingly, there have been no definitive studies of absolute flash detection efficiency for VHF lightning mapping systems, likely due to the difficulty of providing ground-truth information. To date, indirect assessment has led to the conclusion that a properly operating VHF mapping system has nearly 100% DE for cloud and cloud-to-ground flashes within the interior of the network. As described in *Cummins and Murphy* [2009], there have been comparisons [e.g., *Lojou and Cummins*, 2006; *Mazur et al*., 1997] of different types of VHF mapping systems using time-of-arrival and interferometry to geolocate lightning. Those studies show that although different processes within flashes may be preferentially observed by time-of-arrival or interferometric VHF mapping systems, both systems can provide similar flash counts and spatial representations of flashes.

The most common method used to validate satellite-based LLS performance is LLS intercomparison. Examples include assessment of the CG flash performance of OTD using NLDN CG flash data as reference [*Boccippio et al*., 2000] and assessment of total flash DE using VHF mapping data from LMA as reference [*Thomas et al*., 2000]. Also, satellite-based LLS data are sometimes used as reference to examine the total flash detection efficiency of ground-based LLSs [e.g., *Rudlosky and Shea*, 2013; *Rudlosky*, 2014; *Thompson et al*., 2014]. One of the complications of using lightning data provided by low-Earth orbiting satellite-based LLSs as test or reference is the need to track the field of view on a per-second basis. The viewing time for a specific location on the Earth varies with the satellite altitude, and is on the order of a few minutes. Additionally, the emissions detected by ground-based LLSs result from lightning processes that are different than those associated with the emissions detected by satellite-based LLSs as discussed in section 2. Hence, uncertainties related to correlating individual events detected by these LLSs are often large. For example, groups of events having high radiance in satellite-based LLS data sets are not necessarily correlated with lightning events having high peak currents in ground-based LLS data sets [e.g., *Boccippio et al*., 2000; *Thompson et al*., 2014]. In fact, *Thompson et al*. [2014] reported that groups of events having high radiance detected by LIS only had a coincident ground-based LLS-detected lightning event about half of the time. Finally, due to the different nature of the emissions detected by ground-based and satellite-based LLSs (as discussed in section 2), correlation of data from such LLSs may yield lightning events that are exclusive to each data set. As a result, such studies may estimate the correlation percentage between these LLSs [e.g., *Thompson et al*., 2014], rather than the relative detection efficiency of one versus the other.

6. Summary

Ground-based or satellite-based lightning locating systems operating at different frequency ranges detect emissions associated with a variety of different lightning processes. As a result, lightning data provided by such systems often contain complementary information about thunderstorms. Depending upon the frequency range of operation, LLSs may report a variety of processes and characteristics associated with lightning flashes including channel formation, leader pulses, cloud-to-ground return strokes, M-components, ICC pulses, cloud lightning pulses, location, peak current, peak radiated power, and full spatial extent of channels. For all the applications of lightning data, it is critical to understand the information that is provided by various LLSs in order to interpret it correctly and make the best use of it. The performance characteristics of a lightning locating system refer to its ability to detect and report various aspects of lightning discharges. These performance characteristics include (1) detection efficiency (DE) for cloud and cloud-to-ground flashes and cloud-to-ground strokes, (2) location accuracy (LA), (3) polarity and peak current estimation accuracy, (4) lightning type classification accuracy, the ability to differentiate between different processes such as in-cloud pulses and cloud-to-ground strokes, and (5) the ability to minimize false detections. In this paper, we have reviewed the performance characteristics of different kinds of modern ground-based and satellite-based LLSs. A number of techniques for validating the performance characteristics of LLSs exist. While one or a combination of the techniques can be used to evaluate the performance characteristics of an

LLS, it is important to understand the strengths and limitations of the methods used, in order to understand what can and cannot be quantified with certainty about the performance characteristics of any LLS.

Appendix A: False Detections

The performance parameters and validation techniques discussed in sections 4 and 5 are all critical to the proper understanding and utilization of LLS data sets. However, they are all exclusively related to the lightning that is detected. It is also important that an LLS minimize the degree to which it detects and reports anything that is not lightning. However, false detections can have a wide variety of causes and can be very difficult to quantify.

Noise is probably the principal cause of false detections. In ground-based LLSs, noise is often in the form of radio or television broadcast transmissions that lie within the passband of the sensors. Noise can also come from a wide variety of ground-based industrial, transport, and agricultural activities, as well as electrical equipment such as lights, motors, and nearby electric power distribution or transmission lines. In space-based VHF systems such as FORTE, a multitude of ground-based transmitters lies within the field of view at any given time, and because the passbands of the sensor are wide (22 MHz each) [see *Jacobson et al*., 1999], many noise sources are picked up simultaneously. In space-based optical sensors, noise sources are primarily shot noise from bright cloud tops, high-energy particles, nonlightning optical signals such as solar glint reflections from the oceans, and sensor noise [*Boccippio et al*., 2000].

Noise mitigation in LLSs can be as diverse as the LLSs themselves. At the sensor level, various signal characteristics, either in the frequency or time domains or both, may be used to distinguish between lightning and nonlightning signals. Notch filters or other signal processing techniques are sometimes used to remove noise sources coherently from the lightning signals of interest [e.g., *Said et al*., 2010; *Dowden et al*., 2002]. In ground-based LLSs, the central processors can impose a variety of consistency checks between the various sensors during the process of determining the geolocation of a particular event. Alternatively, once events are detected and geolocated, spatiotemporal clustering can be used to identify and remove outliers. The latter method applies equally well to single-sensor satellite-based methods or ground-based multiple-sensor LLSs [e.g., *Boccippio et al*., 2000; *Murphy et al*., 2013].

In addition to noise, false detections can also be due to uncorrected bias errors in the sensor measurements or to poor-quality geolocations of legitimate lightning discharges. For example, if a particular combination of two sensors in a ground-based LLS produces a geolocation in which the estimated random position error is 20 km, and the position lies 15 km away from the remainder of the lightning activity in the parent thunderstorm, then the low-quality position may, in some applications, be regarded as a false detection. To quantify the rate of false detection in this case, however, it is necessary to define the limits of spatial and/or temporal consistency in a cluster of lightning activity associated with a thunderstorm, such that any detection that exceeds those limits can be identified as a false detection.

In ground-based LLSs operating at VHF, particularly those that use the TOA technique, false detections are also generated by small spark-like discharges generated when airplanes fly through ice clouds and create charge separation by collisions with the ice crystals. Such airplane tracks have been discussed by *Boccippio et al*. [2001a] and *Thomas et al*. [2004]. In the latter case, the airplane tracks were utilized as another means of investigating the performance of the LLS, thus converting false detections into an advantage. Airplane tracks are relatively easy to recognize as false detections due to their linear or gently curved organization and their speed of motion, on the order of a couple hundred m/s, which is considerably slower than natural lightning discharge processes.

The majority of the very limited literature on quantifying the false detection rates of LLS uses internetwork comparison as the means of analysis. The World-Wide Lightning Location Network (WWLLN) was compared against the Los Alamos Sferics Array (LASA) by *Jacobson et al*. [2006], who found that 1.7% of the WWLLN events analyzed were uncorrelated with any LASA event within a correlation time window of 200 ms. Although there was said to be some general spatial association with thunderstorm activity when these events were viewed on a map, they were implied to be false detections, a finding that was later questioned by *Abarca et al*. [2010]. *Abreu et al*. [2010] also compared WWLLN data with the Canadian Lightning Detection Network (CLDN), a medium-range LLS operating over the VLF-MF range. They found that 0.05% of WWLLN

events were not coincident with any CLDN event to within 50 km and one hour of any other CLDN events. This much smaller percentage of false detections is clearly due to the use of a storm-scale definition of coincidence by *Abreu et al*. [2010] versus a much stricter event-level definition used by *Jacobson et al*. [2006].

A different approach to the quantification of false detection rate was taken by *Lagouvardos et al*. [2009] and *Poelman et al*. [2013b], although both are still based on network intercomparison studies. In these studies, grids were defined over the regions of coverage of the LLSs and then the number of grid boxes in which the test and reference networks detected zero or nonzero number of events were counted. *Lagouvardos et al*. [2009] considered thunderstorms over southern Germany on a single day, whereas *Poelman et al*. [2013b] included thunderstorms in and around Belgium over many months. The analysis was then done by the 2×2 contingency table method (hits, misses, false alarms, and correct negatives). False alarms were defined as any grid boxes that contained a nonzero count of lightning events from the test network but a zero count from the reference network. By varying which LLS was considered the test and which was considered the reference, in a three-way intercomparison study, *Poelman et al*. [2013b] found false "alarm" (detection) rates between 5% and 17%. In *Lagouvardos et al*. [2009], the corresponding value was 11%, with the ZEUS long-range LLS being the test LLS and LINET serving as the reference. Modern well-calibrated medium range LLSs are expected to have false detections well below 0.1%.

A modeling approach was suggested by *Thomas et al*. [2004] to quantify the false detection rate of the Lightning Mapping Array. There, Monte Carlo simulations were carried out using combinations of six sensors, the minimum required to produce a geolocation in the LMA. The Monte Carlo calculations involved the random introduction of timing errors of 7 μs. The objective was to see how often one of the resulting badly geolocated events would survive the normal quality control based on the chi-square value. The simulation results were not actually given, but the balloon-borne transmitter data that were used to validate the location accuracy of the LMA also yielded the conclusion that no more than 1% of the geolocated sources were likely to be false detections.

It should be noted that false detections can also be ascertained by comparisons of LLS data with radar data and satellite imagery. Overviews of early comparisons of this type, and associated references, were given by *Holle and Lopez* [1993]. Just as with other validation techniques, these approaches require considerable caution. With both radar and satellite data, the temporal resolution is typically much lower than that of the LLS data. The type of thunderstorm also needs to be considered, as squall lines and mesoscale convective systems usually have stratiform precipitation regions that produce lightning but have lower radar reflectivity than the main convective regions of the same storm systems [e.g., *Watson et al*., 1995; *Carey et al*., 2005]. With radar data, beam blockage by terrain is an important consideration [e.g., *Maddox et al*., 2002] and if not taken into account could lead to diagnosing an erroneously high false detection rate on the part of an LLS; maximum column reflectivity, as opposed to a single low elevation angle scan, is a better radar data set to use in complex terrain.

Appendix B: Performance Modeling of LLSs

The validation of LLS performance characteristics such as detection efficiency and location accuracy provides critical information about the performance of an LLS *as it is*. However, that analysis is frequently accompanied by a parallel question about what the performance of the LLS is *expected to be* and, thus, whether the measured performance does or does not satisfy expectations. Models of network performance can therefore be used in conjunction with validation techniques to enhance the understanding of LLS performance. Models are typically used to predict the detection efficiency and location accuracy of LLSs. Other performance characteristics, such as accuracy of peak current estimation or the classification of cloud pulses versus cloud-to-ground return strokes, are either not relevant in the context of modeling or simply too difficult to model well. In this appendix, we focus on detection efficiency (DE) and location accuracy (LA) models.

B1. DE Models

Detection efficiency is equivalent to the probability of detection of lightning discharges by an LLS. In the context of ground-based LLSs, the relevant quantity is the probability of detection by at least the minimum number of sensors required to calculate the geolocation of any particular lightning discharge or discharge process, such as a return stroke, K-change, and preliminary breakdown. In the context of satellite-based

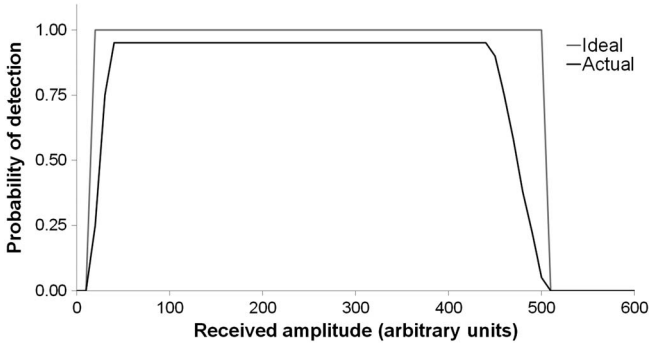

Figure B1. An ideal (grey curve) versus an actual (black curve) sensor probability of detection curve as a function of signal amplitude as seen by a typical sensor.

optical LLS, it is the probability of detecting a signal sufficiently above the background light level without being rejected as a false detection. Here, we review the modeling of DE in ground-based LLSs. Note that the essential elements of DE modeling are addressed in *Pessi et al.* [2009, section 4] but that, in this appendix, we further generalize to include VHF, and we describe the coupling of the location accuracy (LA) model to the DE model.

A ground-based LLS is specified by the positions of the sensors and the sensor characteristics. The essential sensor characteristics are the minimum detectable signal (or threshold) and maximum detectable signal (or saturation), which together specify the dynamic range, and some measure of how a given electric or magnetic field value maps into the sensor dynamic range. The latter quantity is usually simply known as the sensor gain. Given equal dynamic ranges, a sensor with higher gain saturates on nearby lightning signals out to a greater distance than a sensor with lower gain, but conversely, the sensor with higher gain also picks up low-amplitude signals from lightning at greater distances than the sensor with lower gain.

The lightning process to be detected is specified in terms of the naturally occurring distribution of its amplitudes or powers. Preferably, this distribution is specified in terms of a basic physical characteristic of the discharge, such as the peak current of cloud-to-ground return strokes. However, it is often intractable to relate a basic physical characteristic to the signals being measured. A good example is in VHF lightning mapping systems that receive VHF emissions within a particular band. Thus, it is often necessary to rely on measurements made by an LLS to derive the distribution of amplitude or power that is then used in a DE model. When this is necessary, obviously the distribution should be derived from a well-characterized LLS and only in the region where that LLS has high detection efficiency.

The signals emitted by the discharge process to be modeled are then mapped to the spatial distribution of sensors in the LLS via a propagation model, taking into account issues such as ground conductivity (in LF, VLF), reflection of signals from the ionosphere (VLF), or blockage of signals by terrain features and buildings (VHF). Once the signals coming from a particular discharge process are mapped to the sensor locations via the propagation model, the signal levels are then mapped to the sensor characteristics discussed above.

Ideally, each sensor in a ground-based LLS has perfect probability of detection at all amplitudes within its dynamic range, as illustrated by the grey curve in Figure B1. In practice, however, a typical sensor has a probability of detection that varies slightly with signal-to-noise ratio near the threshold. Thus, the probability of detection does not rise immediately at the sensor threshold but rather looks more like the black curve in Figure B1. Similarly, the cutoff at saturation is not sharp either. For example, a sensor that includes magnetic direction finding may begin to report saturation when only one of the two MDF channels reaches saturation, which in turn depends on azimuth as well as the source signal amplitude. The net effect, aggregated over all azimuths, is a slower fall-off in probability of detection rather than a sharp cutoff at saturation, again shown by the black curve in Figure B1. Finally, although most modern digital sensors have no dead time, some older sensors do, and real sensor sites are always affected to some degree by noise and, over time, by power and communications interruptions. Therefore, there is a practical upper limit to probability of detection even within a sensor's dynamic range. This can be modeled simply by reducing the maximum probability of detection to something less than 1.0 in the modeled curve, as shown in Figure B1.

In some DE modeling studies [*Naccarato and Pinto*, 2009; *CIGRE*, 2009; *Chen et al*., 2013], the sensor probability of detection is represented as a function of distance rather than received signal amplitude. This representation

convolves the sensor characteristics with the propagation model. The distribution of source amplitudes can still be handled as a separate input, as in *CIGRE* [2009], but in some cases [*Naccarato and Pinto*, 2009], the sensor probability of detection curve is also convolved with the source amplitude distribution, and thus, the model is rigidly bound to both the sensor and discharge characteristics. In addition, if the probability of detection characteristic is derived directly from the LLS by monitoring the relative frequency of contribution of each sensor, then the sensor probability of detection curve is also convolved directly with LLS performance, including any local or regional degradation. For example, the loss of a particular sensor due, e.g., to an extended communication outage, reduces the DE in a region around that sensor. Other sensors that cover the same region then have higher relative DE because they necessarily have to do most or all of the detection in that region, and any probability of detection curves derived from the relative contributions of those sensors may be too optimistic.

The essence of the DE model is then to compute the overall probabilities of detection by any combination of sensors in the LLS that is capable of determining a geolocation. This overall probability must involve integration over the natural source amplitude distribution described above. Equation (B1) summarizes this for combinations of two sensors, applicable to LLSs where a minimum of two sensors is capable of performing geolocation; similar integrations are performed over all possible combinations of sensors capable of performing geolocation.

$$P(\textit{combos of } 2,\ \textit{lat},\ \textit{lon}) = \int_{A_{\min}}^{A_{\max}} p_A(x)\left[\sum_{i,j} p_d(i,\ \Pr(\textit{lat},\textit{lon},i,x))\ p_d(j,\ \Pr(\textit{lat},\textit{lon},j,x))\prod_{k\neq i,k\neq j}(1-\ p_d(k,\ \Pr(\textit{lat},\textit{lon},k,x)))\right] \mathrm{d}x \tag{B1}$$

Here, a lightning discharge is assumed to occur at a location given by *lat*, *lon*. The function $p_A(x)$ is the probability of amplitude x from the natural distribution of amplitudes or powers, p_A, which extends from $A_{\min}$ to $A_{\max}$. The function p_d is a sensor probability of detection, taken from a curve such as that shown in Figure B1. Its value is dependent upon the mapping of amplitude value x from the lightning at *lat*, *lon* to the sensor position via the signal propagation model, represented in this equation by *Pr*(*lat*, *lon*, *i*, *x*), where *i* is a sensor index.

The overall DE at the point *lat*, *lon* is obtained by summing over the combinations of 2, 3, 4, …, *n* sensors in the LLS. In practice, if the LLS contains more than 10 sensors, the combinations of 10 or more contributing sensors from a larger set of sensors, most of which are typically at large distance from the point *lat*, *lon*, add very little to the DE model other than large computational expense. Thus, to maintain practical computation time, it is reasonable to select the closest 10 or so sensors to each point *lat*, *lon* and compute just the possible combinations of those sensors. By tracking the overall probabilities of detection by combinations of 2, 3, 4, …, *n* sensors, the model of the expected distribution of the NSR is automatically computed along with the overall DE at any given point *lat*, *lon*. Thus, Figures 2a and 2b are readily derivable from a single model.

B2. LA Models

The random error in the position estimates provided by ground-based LLSs is described by a statistical confidence region having an elliptical shape in general. The elliptical shape derives from the shapes of the contours of constant differential in the cost function that is minimized in the nonlinear modeling process. That cost function typically takes the form of a sum of squares and obeys a chi-square distribution, and thus, its value is often referred to simply as the chi-square value associated with each lightning position. The contours of chi-square differential relative to the global minimum (ideally; or a local minimum in a nonideal case) mapped onto the two-dimensional latitude, longitude space form ellipses. These ellipses map to statistical confidence levels. Thus, it is common to hear the term "error ellipse" or "confidence ellipse" used to refer to the estimate of random position error associated with LLS data.

The relationship between the contours of chi-square differential and the statistical confidence intervals, and the method of determining the sizes of the confidence regions, have been described succinctly in the nonlinear modeling section of *Press et al*. [2007, Chap. 15, 3rd ed.]. This relationship fundamentally involves the Hessian, which is built from the derivatives of measured data values (e.g., time and/or angle measurements from multiple sensors) with respect to the parameters of the nonlinear model (in the spatial dimensions, latitude and longitude). The terms of the Hessian are also weighted by the variances of the

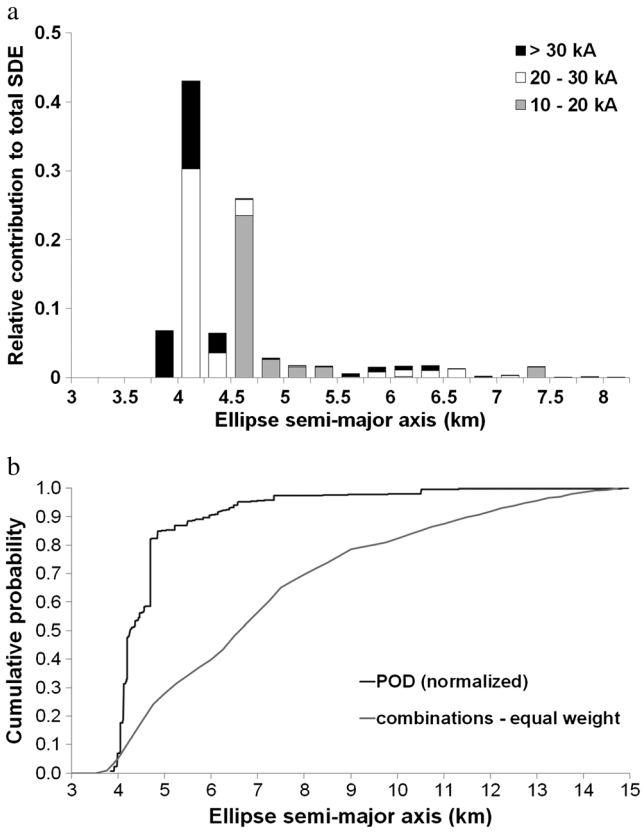

Figure B2. (a) Distribution of the modeled confidence ellipse semimajor axis lengths, at the position marked "B" in Figure 2a in the body of the paper. Each bin contains the relative contributions to the total stroke detection efficiency (SDE). (b) The black curve shows the cumulative probability of detection (POD) derived from Figure B2a. The grey curve shows the cumulative probability distribution that does not take the contributing probabilities of detection into account.

measured data values. The derivatives that go into the Hessian depend strongly on the positions of the sensors with respect to the lightning whose positional parameters are to be estimated from the measurements. The Hessian thus encapsulates the positions of sensors with respect to the lightning and the random errors in the measurements provided by each sensor. These pieces of information —sensor positions relative to lightning and random measurement errors—are the fundamental building blocks of an LA model.

Because of the positional dependence of the derivatives going into the Hessian, the values in the Hessian for each lightning discharge are also dependent on the specific combination of sensors that detect the discharge. The positional dependence with respect to a single combination of three sensors is illustrated in *Cummins and Murphy* [2009]. Thus, LA models are combinatorial, just as the DE models discussed in the previous section, and the output is a distribution of the confidence region sizes produced by all sensor combinations. In order to produce a map of representative location accuracies over the entire area of coverage of an LLS, it is customary to take a single value, usually the median, from that distribution of all confidence region sizes. However, in doing that, it is critical to take into account the fact that not all sensor combinations are equally likely to detect, and thus, the median must be based on the halfway point in the cumulative probability of detection. In other words, the ellipse values are ranked by the probabilities of stroke detection of the specific sensor combinations that generate them. Figures B2a and B2b illustrate these points, using the point marked B in Figure 2a. Figure B2a shows the distribution of the modeled confidence ellipse semimajor axis lengths with each axis-length bin containing the relative contribution to the total stroke DE. The bars in Figure B2a are color-coded by three ranges of peak current to illustrate the fact that smaller ellipses are associated with higher peak currents. This is because there is a higher probability of having all or nearly all sensors contributing at the higher peak currents. In Figure B2b, the black curve shows the cumulative probability density derived from the histogram in Figure B2a together with a second cumulative probability distribution that does not take the contributing probabilities of detection into account (grey curve). We see that half of the total detection efficiency is accounted for by sensor combinations whose semimajor axis lengths are below 4.25 km, while the median is much larger, 6.6 km, if the probability of detection information is not considered. The former value, 4.25 km, is the value that truly represents the median location accuracy provided at this location (point B in Figure 2a) well outside the perimeter of the LLS.

It is also worth noting that a coupled LA-DE model can be used to provide appropriate feedback between LA and DE in order to produce DE estimates that are more representative of reality around the periphery of ground-based LLSs. In practice, lightning positions with very large confidence ellipses are typically rejected in

LLS data sets because of their poor quality. Such positions occur mainly outside the perimeter of the LLS sensors. The limiting value of ellipse size used in an LLS can also be used to zero out the DE values of any combinations of sensors whose modeled LA exceeds the limit. This then leads to lower, but more realistic, DE estimates in regions outside the LLS perimeter. We have, in fact, applied this practice in the generation of the stroke DE and associated NSR distributions in Figures 2a and 2b and in Figures B2a and B2b discussed. The maximum semimajor axis length in these model runs was set to 15 km.

The coupling between LA and DE, and the application of a realistic maximum LA value, leads to interesting behavior in the distribution of NSR, which can be used in network self-reference studies, as described in section 5.1. Specifically, in areas well outside the perimeter of a network, such as points C and D in Figure 2a, one might expect that the minimum NSR required to geolocate a stroke would eventually become the most probable value of NSR. In fact, however, as the distance outside the network increases, the error ellipses associated with most, and eventually all, of the minimum-NSR combinations of sensors become so large that these combinations are rejected. Thus, the NSR distribution converges toward a large peak at a value that is not the absolute minimum, as illustrated for point D of Figure 2a. When the absolute minimum NSR is 2, as in the example network used here, then the NSR distribution is also affected by the directional location accuracy effects near the lines joining pairs of sensors, as mentioned in sections 3.2 and 3.4. Additionally, if there are points outside of a network where even more sensors are nearly equidistant from the points in question, then the NSR distribution tends to converge toward an even larger number at those points. A good example of such a situation is a concave section of coastline with sensors that are approximately evenly spaced along the coast. In that case, even points that are a couple hundred km offshore may have NSR distributions that peak at, say, 4–5, even though the minimum number of sensors required to geolocate is only 2.

Acknowledgments
To access the data in this paper, please contact the corresponding author. The authors would like to thank H. Christian, S. Goodman, and two anonymous reviewers for their comments on the paper.

References

Abarca, S., K. Corbosiero, and T. Galarneau (2010), An evaluation of the Worldwide Lightning Location Network (WWLLN) using the National Lightning Detection Network (NLDN) as ground truth, *J. Geophys. Res.*, *115*, D18206, doi:10.1029/2009JD013411.

Abreu, D., D. Chandan, R. Holzworth, and K. Strong (2010), A performance assessment of the World Wide Lightning Location Network (WWLLN) via comparison with the Canadian Lightning Detection Network (CLDN), *Atmos. Meas. Tech. Discuss.*, *3*(2), 1861–1887.

Akita, M., S. Yoshida, Y. Nakamura, T. Morimoto, T. Ushio, Z. Kawasaki, and D. Wang (2011), Effects of charge distribution in thunderstorms on lightning propagation paths in Darwin, Australia, *J. Atmos. Sci.*, *68*(4), 719–726.

Ballarotti, M. G., M. M. F. Saba, and O. Pinto Jr. (2006), A new performance evaluation of the Brazilian Lightning Location System (RINDAT) based on high-speed camera observations of natural negative ground flashes, *19th International Lightning Detection Conference & 1st International Lightning Meteorology Conference*, Tucson, Ariz.

Berger, K., R. B. Anderson, and H. Kroninger (1975), Parameters of lightning flashes, *Electra*, *41*, 23–37.

Bermudez, J. L., F. Rachidi, W. Janischewskyj, V. Shostak, M. Rubinstein, D. Pavanello, A. M. Hussein, J. S. Chang, and M. Paolone (2007), Determination of lightning currents from far electromagnetic fields: Effect of a strike object, *J. Electrost.*, *65*, 289–295, doi:10.1016/j.elstat.2006.09.007.

Biagi, C. J., K. L. Cummins, K. Kehoe, and E. P. Krider (2007), National lightning detection network (NLDN) performance in southern Arizona, Texas, and Oklahoma in 2003–2004, *J. Geophys. Res.*, *112*, D05208, doi:10.1029/2006JD007341.

Boccippio, D., W. Koshak, R. Blakeslee, K. Driscoll, D. Mach, D. Buechler, W. Boeck, H. Christian, and S. Goodman (2000), The Optical Transient Detector (OTD): Instrument characteristics and cross-sensor validation, *J. Atmos. Oceanic Technol.*, *17*(4), 441–458.

Boccippio, D., S. Heckman, and S. Goodman (2001a), A diagnostic analysis of the Kennedy Space Center LDAR network: 1. Data characteristics, *J. Geophys. Res.*, *106*(D5), 4769–4786, doi:10.1029/2000JD900687.

Boccippio, D., K. Cummins, H. Christian, and S. Goodman (2001b), Combined satellite- and surface-based estimation of the intracloud-cloud-to-ground lightning ratio over the continental United States, *Mon. Weather Rev.*, *129*(1), 108–122.

Boccippio, D., W. Koshak, and R. Blakeslee (2002), Performance assessment of the Optical Transient Detector and Lightning Imaging Sensor. Part I: Predicted diurnal variability, *J. Atmos. Oceanic Technol.*, *19*(9), 1318–1332.

Carey, L., M. Murphy, T. McCormick, and N. Demetriades (2005), Lightning location relative to storm structure in a leading-line, trailing-stratiform mesoscale convective system, *J. Geophys. Res.*, *110*, D03105, doi:10.1029/2003JD004371.

Cecil, D., D. Buechler, and R. Blakeslee (2014), Gridded lightning climatology from TRMM-LIS and OTD: Dataset description, *Atmos. Res.*, *135*, 404–414.

Chen, L., Y. Zhang, W. Lu, D. Zheng, Y. Zhang, S. Chen, and Z. Huang (2012), Performance evaluation for a lightning location system based on observations of artificially triggered lightning and natural lightning flashes, *J. Atmos. Oceanic Technol.*, *29*(12), 1835–1844, doi:10.1175/JTECH-D-12-00028.1.

Chen, M., D. Zheng, Y. Du, and Y. Zhang (2013), A statistical method for evaluating detection efficiency of lightning location network and its application, *Atmos. Res.*, *128*, 13–23.

Christian, H., R. Blakeslee, and S. Goodman (1989), The detection of lightning from geostationary orbit, *J. Geophys. Res.*, *94*(D11), 13,329–13,337, doi:10.1029/JD094iD11p13329.

Christian, H., et al. (2003), Global frequency and distribution of lightning as observed from space by the Optical Transient Detector, *J. Geophys. Res.*, *108*(D1), 4005, doi:10.1029/2002JD002347.

Christian, H. J., K. T. Driscoll, S. J. Goodman, R. J. Blakeslee, D. A. Mach, and D. E. Buechler (1996), The Optical Transient Detector (OTD), in *10th Intl. Conf. on Atmospheric Electricity*, pp. 368–371, ICAE, Osaka, Japan.

Christian, H. J., et al. (1999), The Lightning Imaging Sensor, in *11th Intl. Conf. on Atmospheric Electricity*, pp. 746–749, ICAE, Guntersville, Ala.

Chronis, T. G., and E. N. Anagnostou (2006), Evaluation of a long-range lightning detection network with receivers in Europe and Africa, *IEEE Trans. Geosci. Remote Sens.*, *44*(6), 1504–1510.

CIGRE (2009), Cloud-to-ground parameters derived from lightning location systems: The effects of system performance, *CIGRE C4.404A*.
Cooray, V. (1987), Effects of propagation on the return stroke radiation fields, *Radio Sci.*, *22*(5), 757–768, doi:10.1029/RS022i005p00757.
Cramer, J. A., and K. L. Cummins (2014), Evaluating location accuracy of lightning location networks using tall towers, in *23rd International Lightning Detection Conference & 5th International Lightning Meteorology Conference*, Vaisala Inc., Tucson, Ariz.
Cummins, K., and M. Murphy (2009), An overview of lightning locating systems: History, techniques, and data uses, with an in-depth look at the US NLDN, *IEEE Trans. Electromag. Compat.*, *51*(3), 499–518, doi:10.1109/TEMC.2009.2023450.
Cummins, K., M. Murphy, E. Bardo, W. Hiscox, R. Pyle, and A. Pifer (1998), A combined TOA/MDF technology upgrade of the US National Lightning Detection Network, *J. Geophys. Res.*, *103*(D8), 9035–9044, doi:10.1029/98JD00153.
Cummer, S. A., Y. Zhai, W. Hu, D. M. Smith, L. I. Lopez, and M. A. Stanley (2005), Measurements and implications of the relationship between lightning and terrestrial gamma ray flashes, *Geophys. Res. Lett.*, *32*, L08811, doi:10.1029/2005GL022778.
Cummer, S. A., G. Lu, M. S. Briggs, V. Connaughton, S. Xiong, G. J. Fishman, and J. R. Dwyer (2011), The lightning–TGF relationship on microsecond timescales, *Geophys. Res. Lett.*, *38*, L14810, doi:10.1029/2011GL048099.
Cummins, K. L., M. J. Murphy, J. A. Cramer, W. Scheftic, N. Demetriades, and A. Nag (2010), Location accuracy improvements using propagation corrections: a case study of the U.S. National Lightning Detection Network, *21st Intl. Lightning Detection Conf.*, Orlando, Fla.
Cummins, K. L., D. Zhang, M. G. Quick, A. C. Garolera, and J. Myers (2014), Performance of the U.S. National Lightning Detection Network during the Kansas Windfarm 2012 and 2013 field programs, in *23rd International Lightning Detection Conference & 5th International Lightning Meteorology Conference*, Vaisala Inc., Tucson, Ariz.
Diendorfer, G. (2010), LLS performance validation using lightning to towers, in *21st International Lightning Detection Conference* & *3rd International Lightning Meteorology Conference*, Orlando, Fla.
Diendorfer, G., M. Mair, W. Schulz, and W. Hadrian (2000a), Lightning current measurements in Austria—Experimental setup and first results, in *25th Intl. Conf. on Lightning Protection*, pp. 44–47, ICLP Centre, Rhodes, Greece.
Diendorfer, G., W. Schulz, and M. Mair (2000b), Evaluation of a LLS based on lightning strikes to an instrumented tower, in *16th International Lightning Detection Conference*, Tucson, Ariz.
Dowden, R. L., J. B. Brundell, and C. J. Rodger (2002), VLF lightning location by time of group arrival (TOGA) at multiple sites, *J. Atmos. Sol. Terr. Phys.*, *64*(7), 817–830, doi:10.1016/S1364-6826(02)00085-8.
Eriksson, A. J., and D. V. Meal (1984), The incidence of direct lightning strikes to structures and overhead lines, in *IEE-Conference on Lightning and Power Systems*, IEE-Conference Publ., vol. 236, pp. 67–71, IEE, London.
Finke, U., J. Grandell, E. Defer, and H. Höller (2010), The lightning imager (LI) on MTG—Scientific studies and developments, Abstract #AE24A-03 presented at 2010 Fall Meeting, AGU, San Francisco, Calif., 11–17 Dec.
Goodman, S. J., H. J. Christian, and W. D. Rust (1988), A comparison of the optical pulse characteristics of intracloud and cloud-to-ground lightning as observed above clouds, *J. Appl. Meteorol.*, *27*, 1369–1381, doi:10.1175/1520-0450(1988)027<1369:ACOTOP>2.0.CO;2.
Goodman, S. J., et al. (2013), The GOES-R Geostationary Lightning Mapper (GLM), *Atmos. Res.*, *125*, 34–49.
Grandell, J., et al. (2010), EUMETSAT Meteosat Third Generation (MTG) lightning imager: From mission requirements to product development, Abstract #AE21A–0257 presented at 2010 Fall Meeting, AGU, San Francisco, Calif., 11–17 Dec.
Heckman, S., and C. Liu (2010), The application of total lightning detection and cell tracking for severe weather prediction, in *GROUND'2010 & 4th LPE*, pp. 234–240, SBRAI, Salvador, Brazil.
Holle, R. L., and R. E. Lopez (1993), Overview of real-time lightning detection systems and their meteorological uses, *NOAA Tech. Memo. ERL NSSL-102*, National Severe Storms Laboratory, Norman, Okla.
Holler, H., H.-D. Betz, U. Finke, and K. Schmidt (2012), Lightning detection, in *Atmospheric Physics, Background – Methods – Trends*, edited by U. Schumann, chap. 20, pp. 331–346, Springer, Berlin.
Honma, N., K. L. Cummins, M. J. Murphy, A. E. Pifer, and T. S. Rogers (2013), Improved lightning locations in the Tohoku Region of Japan using propagation and waveform onset corrections, *IEEJ Trans. Power Energy*, *133*(2), 195–202, doi:10.1541/ieejpes.133.195.
Horner, F. (1964), Radio noise from thunderstorms, in *Advances in Radio Research*, vol. 2, pp. 121–204, edited by J. A. Saxton, Academic Press, New York.
Hutchins, M., R. Holzworth, C. Rodger, and J. Brundell (2012a), Far-field power of lightning strokes as measured by the World Wide Lightning Location Network, *J. Atmos. Oceanic Technol.*, *29*(8), 1102–1110.
Hutchins, M., R. Holzworth, J. Brundell, and C. Rodger (2012b), Relative detection efficiency of the world wide lightning location network, *Radio Sci.*, *47*, RS6005, doi:10.1029/2012RS005049.
Idone, V. P., D. A. Davis, P. K. Moore, Y. Wang, R. W. Henderson, M. Ries, and P. F. Jamason (1998a), Performance evaluation of the U.S. National Lightning Detection Network in eastern New York: 1. Detection efficency, *J. Geophys. Res.*, *103*(D8), 9045–9055, doi:10.1029/98JD00154.
Idone, V. P., D. A. Davis, P. K. Moore, Y. Wang, R. W. Henderson, M. Ries, and P. F. Jamason (1998b), Performance evaluation of the U.S. National Lightning Detection Network in eastern New York: 2. Location accuracy, *J. Geophys. Res.*, *103*(D8), 9057–9069, doi:10.1029/98JD00155.
Jacobson, A., S. Knox, R. Franz, and D. Enemark (1999), FORTE observations of lightning radio-frequency signatures: Capabilities and basic results, *Radio Sci.*, *34*(2), 337–354, doi:10.1029/1998RS900043.
Jacobson, A., X. Shao, and R. Holzworth (2011), Satellite triangulation of thunderstorms, from fading radio fields synchronously recorded on two orthogonal antennas, *Radio Sci.*, *46*, RS6012, doi:10.1029/2011RS004783.
Jacobson, A. R., R. Holzworth, J. Harlin, R. Dowden, and E. Lay (2006), Performance assessment of the Worldwide Lightning Location Network (WWLLN) using the Los Alamos Sferic Array (LASA) as ground truth, *J. Atmos. Oceanic Technol.*, *23*, 1082–1092.
Jerauld, J., V. Rakov, M. Uman, K. Rambo, D. Jordan, K. Cummins, and J. Cramer (2005), An evaluation of the performance characteristics of the US National Lightning Detection Network in Florida using rocket-triggered lightning, *J. Geophys. Res.*, *110*, D19106, doi:10.1029/2005JD005924.
Kirkland, M. W., D. M. Suszcynsky, J. L. L. Guillen, and J. L. Green (2001), Optical observations of terrestrial lightning by the FORTE satellite photodiode, *J. Geophys. Res.*, *106*(D24), 33,499–33,509, doi:10.1029/2000JD000190.
Kosarev, E., V. Zatsepin, and A. Mitrofanov (1970), Ultrahigh frequency radiation from lightnings, *J. Geophys. Res.*, *75*(36), 7524–7530, doi:10.1029/JC075i036p07524.
Koshak, W. J. (2010), Optical characteristics of OTD flashes and the implications for flash-type discrimination, *J. Atmos. Oceanic Technol.*, *27*, 1822–1838.
Koshak, W. J., and R. J. Solakiewicz (2011), Retrieving the fraction of ground flashes from satellite lightning imager data using CONUS-based optical statistics, *J. Atmos. Oceanic Technol.*, *28*, 459–473.
Krider, E. P., R. C. Noggle, and M. A. Uman (1976), A gated, wideband magnetic direction finder for lightning return strokes, *J. Appl. Meteorol.*, *15*(3), 301–306.

Lagouvardos, K., V. Kotroni, H. Betz, and K. Schmidt (2009), A comparison of lightning data provided by ZEUS and LINET networks over Western Europe, *Nat. Hazards Earth Syst. Sci.*, *9*(5), 1713–1717.

Lojou, J.-Y., and K. L. Cummins (2006), Total lightning mapping using both VHF interferometry and time-of-arrival techniques, in *19th Intl. Lightning Detection Conf.*, Tucson, Ariz.

Lojou, J.-Y., M. J. Murphy, R. L. Holle, and N. W. S. Demetriades (2009), Nowcasting of thunderstorms using VHF measurements, in *Lightning: Principles, Instruments, and Application, Review of Modern Lightning Research*, chap. 11, edited by H. D. Betz, U. Schumann, and P. Laroche, pp. 253–270, Springer, Dordrecht, Netherlands.

Lugrin, G., N. Parra, F. Rachidi, M. Rubinstein, and G. Diendorfer (2014), On the location of lightning discharges using time reversal of electromagnetic fields, *IEEE Trans. Electromagn. Compat.*, *56*(1), 149–158.

Lyu, F., S. A. Cummer, J. L. Weinert, L. E. McTague, R. Solanki, and J. Barrett (2014), Development and application of a low frequency near-field interferometric-TOA 3D Lightning Mapping Array, Abstract AE24A-01, presented at 2014 Fall Meeting, AGU, San Francisco, Calif., 15–19 Dec.

Mach, D., H. Christian, R. Blakeslee, D. Boccippio, S. Goodman, and W. Boeck (2007), Performance assessment of the Optical Transient Detector and Lightning Imaging Sensor, *J. Geophys. Res.*, *112*, D09210, doi:10.1029/2006JD007787.

Maddox, R., J. Zhang, J. Gourley, and K. Howard (2002), Weather radar coverage over the contiguous United States, *Weather Forecasting*, *17*(4), 927–934.

Malan, D. (1963), *Physics of Lightning*, 1st ed., English Univ. Press, London.

Mallick, S., V. A. Rakov, T. Ngin, W. R. Gamerota, J. T. Pilkey, J. D. Hill, M. A. Uman, D. M. Hordan, M. L. Hutchins, and R. H. Holzworth (2014a), Evaluation of the WWLLN performance characteristics using rocket-triggered lightning data, in *Intl. Conf. on Grounding and Earthing / 6th Intl. Conf. on Lightning Physics and Effects*, Manaus, Brazil.

Mallick, S., V. Rakov, T. Ngin, W. Gamerota, J. Pilkey, J. Hill, M. Uman, D. Jordan, A. Nag, and R. Said (2014b), Evaluation of the GLD360 performance characteristics using rocket-and-wire triggered lightning data, *Geophys. Res. Lett.*, *41*, 3636–3642, doi:10.1002/2014GL059920.

Mallick, S., et al. (2014c), Performance characteristics of the NLDN for return strokes and pulses superimposed on steady currents, based on rocket-triggered lightning data acquired in Florida in 2004–2012, *J. Geophys. Res. Atmos.*, *119*, 3825–3856, doi:10.1002/2013JD021401.

Mallick, S., et al. (2014d), Performance characteristics of the ENTLN evaluated using rocket-triggered lightning data, *Electr. Power Syst. Res.*, *118*, 15–28, doi:10.1016/j.epsr.2014.06.007, in press.

Mallick, S., V. A. Rakov, T. Ngin, W. R. Gamerota, J. T. Pilkey, J. D. Hill, M. A. Uman, D. M. Jordan, J. A. Cramer, and A. Nag (2014e), An update on the performance characteristics of the NLDN, in *23rd International Lightning Detection Conference & 5th International Lightning Meteorology Conference*, Vaisala Inc., Tucson, Ariz.

Mardiana, R., and Z. Kawasaki (2000), Broadband radio interferometers utilizing sequential triggering technique for locating fast electromagnetic sources emitted from lightning, *IEEE Trans. Instrum. Meas.*, *49*(2), 376–381.

Mata, C. T., J. D. Hill, A. G. Mata, and K. L. Cummins (2014), Evaluation of the performance characteristics of CGLSS and NLDN based on two years of ground-truth data from launch complex 39B, Kennedy Space Center, Florida, in *23rd International Lightning Detection Conference & 5th International Lightning Meteorology Conference*, Vaisala Inc., Tucson, Ariz.

Mazur, V., E. Williams, R. Boldi, L. Maier, and D. E. Proctor (1997), Initial comparison of lightning mapping with operational time-of-arrival and interferometric techniques, *J. Geophys. Res.*, *102*(D10), 11,071–11,085, doi:10.1029/97JD00174.

Medici, G., K. L. Cummins, W. J. Koshak, S. D. Rudlosky, R. J. Blakeslee, S. J. Goodman, and D. J. Cecil (2015), The intra-cloud lightning fraction in the contiguous United States, in *Seventh Conference on the Meteorological Applications of Lightning Data*, Am. Meteorol. Soc., Phoenix, 4–8 Jan.

Morales, C. A., J. R. Neves, E. M. Anselmo, L. S. Camara, W. Barreto, V. Paiva, and R. L. Holle (2014), 8 years of Sferics Timing And Ranging NETwork – STARNET: A lightning climatology over South America, in *23rd International Lightning Detection Conference & 5th International Lightning Meteorology Conference*, Am. Meteorol. Soc., Tucson, Ariz.

Morimoto, T., H. Kikuchi, M. Sato, M. Suzuki, A. Yamazaki, and T. Ushio (2011), VHF lightning observations on JEM-GLIMS mission—Gradual approach to realize space-borne VHF broadband digital interferometer, *IEEJ Trans. Fundam. Mater.*, *131*, 977–982.

Morimoto, T., H. Kikuchi, M. Sato, T. Ushio, A. Yamazaki, M. Suzuki, and Z. Kawasaki (2014), VHF lightning observations by digital interferometry from ISS/JEM-GLIMS, in *XV International Conference on Atmospheric Electricity*, International Commission on Atmospheric Electricity, Norman, Okla., 15–20 June.

Murphy, M., and A. Nag (2015), Cloud lightning performance and climatology of the U.S. based on the upgraded U.S. National Lightning Detection Network, in *Seventh Conference on the Meteorological Applications of Lightning Data*, paper 8.4, Am. Meteorol. Soc., Phoenix, Ariz., 4–8 Jan.

Murphy, M. J. (2006), When flash algorithms go bad, in *19th International Lightning Detection Conference & 1st International Lightning Meteorology Conference*, Tucson, Ariz.

Murphy, M. J., A. Nag, J.-Y. Lojou, and R. K. Said (2013), Preliminary analysis of the Vaisala TLS200 network deployed during the CHUVA campaign, in *Sixth Conference on the Meteorological Applications of Lightning Data*, Am. Meteorol. Soc., Austin, Tex., 5–10 Jan.

Murphy, M. J., A. Nag, J. A. Cramer, and A. E. Pifer (2014), Enhanced cloud lightning performance of the U.S. National Lightning Detection Network following the 2013 upgrade, in *23rd International Lightning Detection Conference & 5th International Lightning Meteorology Conference*, Vaisala Inc., Tucson, Ariz.

Naccarato, K., and O. Pinto Jr. (2009), Improvements in the detection efficiency model for the Brazilian lightning detection network (BrasilDAT), *Atmos. Res.*, *91*(2), 546–563.

Nag, A., and V. A. Rakov (2014), Parameters of electric field waveforms produced by positive lightning return strokes, *IEEE Trans. Electromagn. Compat.*, *56*(4), 932–939, doi:10.1109/TEMC.2013.2293628.

Nag, A., V. Rakov, W. Schulz, M. Saba, R. Thottappillil, C. Biagi, A. Oliveira Filho, A. Kafri, N. Theethayi, and T. Gotschl (2008), First versus subsequent return-stroke current and field peaks in negative cloud-to-ground lightning discharges, *J. Geophys. Res.*, *113*, D19112, doi:10.1029/2007JD009729.

Nag, A., V. Rakov, D. Tsalikis, and J. Cramer (2010), On phenomenology of compact intracloud lightning discharges, *J. Geophys. Res.*, *115*, D14115, doi:10.1029/2009JD012957.

Nag, A., et al. (2011a), Evaluation of US National Lightning Detection Network performance characteristics using rocket-triggered lightning data acquired in 2004–2009, *J. Geophys. Res.*, *116*, D02123, doi:10.1029/2010JD014929.

Nag, A., V. Rakov, and J. Cramer (2011b), Remote measurements of currents in cloud lightning discharges, *IEEE Trans. Electromagn. Compat.*, *53*(2), 407–413.

Nag, A., M. J. Murphy, K. L. Cummins, A. E. Pifer, and J. A. Cramer (2014), Recent evolution of the U.S. National Lightning Detection Network, in *23rd International Lightning Detection Conference & 5th International Lightning Meteorology Conference*, Vaisala Inc., Tucson, Ariz.

Norton, K. (1937), The propagation of radio waves over the surface of the Earth and in the upper atmosphere, *Proc. Inst. Radio Eng.*, *25*(9), 1203–1236.
Oetzel, G. N., and E. T. Pierce (1969), Radio emissions from close lightning, in *Planetary Electrodynamics*, Proc. of the 4th Intl. Conf. on the Universal Aspects of Atmos. Electricity, vol. 1, edited by S. C. Coroniti and J. Hughes, Gordon and Breach, New York.
Orville, R., and R. Henderson (1986), Global distribution of midnight lightning: September 1977 to August 1978, *Mon. Weather Rev.*, *114*(12), 2640–2653.
Orville, R., G. Huffines, W. Burrows, R. Holle, and K. Cummins (2002), The north American lightning detection network (NALDN)—First results: 1998–2000, *Mon. Weather Rev.*, *130*(8), 2098–2109.
Orville, R., G. Huffines, W. Burrows, and K. Cummins (2011), The North American lightning detection network (NALDN)-Analysis of flash data: 2001–09, *Mon. Weather Rev.*, *139*(5), 1305–1322.
Pavanello, D., et al. (2007a), On return stroke currents and remote electromagnetic fields associated with lightning strikes to tall structures: 2. Experiment and model validation, *J. Geophys. Res.*, *112*, D13101, doi:10.1029/2006JD007959.
Pavanello, D., F. Rachidi, M. Rubinstein, J. Bermudez, W. Janischewskyj, V. Shostak, C. Nucci, A. Hussein, and J. Chang (2007b), On return stroke currents and remote electromagnetic fields associated with lightning strikes to tall structures: 1. Computational models, *J. Geophys. Res.*, *112*, D13122, doi:10.1029/2006JD007958.
Pavanello, D., F. Rachidi, W. Janischewskyj, M. Rubinstein, V. Shostak, C. A. Nucci, K. L. Cummins, A. M. Hussein, and J. S. Chang (2009), On the current peak estimates provided by lightning detection networks for lightning return strokes to tall towers, *IEEE Trans. Electromagn. Compat.*, *51*(3), 453–458.
Pessi, A., S. Businger, K. Cummins, N. Demetriades, M. Murphy, and B. Pifer (2009), Development of a long-range lightning detection network for the Pacific: Construction, calibration, and performance*, *J. Atmos. Oceanic Technol.*, *26*(2), 145–166.
Pichler, H., G. Diendorfer, and M. Mair (2010), Some parameters of correlated current and radiated field pulses from lightning to the Gaisberg Tower, *IEEJ Trans. Electr. Electr. Eng.*, *5*(1), 8–13.
Pinto, O., Jr., I. R. C. A. Pinto, M. M. F. Saba, and K. P. Naccarato (2009), Cloud-to-ground lightning observations in Brazil, in *Lightning: Principles, Instruments, and Application, Review of Modern Lightning Research*, edited by H. D. Betz, U. Schumann, and P. Laroche, chap. 9, pp. 209–229, Springer, Dordrecht, Netherlands.
Poelman, D. R., W. Schulz, and C. Vergeiner (2013a), Performance characteristics of distinct lightning detection networks covering Belgium, *J. Atmos. Oceanic Technol.*, *30*, 942–951, doi: 10.1175/JTECH-D-12-00162.1.
Poelman, D. R., F. Honoré, G. Anderson, and S. Pedeboy (2013b), Comparing a regional, subcontintental, and long-range lightning location system over the Benelux and France, *J. Atmos. Oceanic Technol.*, *30*, 2394–2405, doi:10.1175/JTECH-D-12-00263.1.
Pohjola, H., and A. Makela (2013), The comparison of GLD360 and EUCLID lightning location systems in Europe, *Atmos. Res.*, *123*, 117–128.
Press, W. H., B. P. Flannery, S. A. Teukolsky, and W. T. Vetterling (2007), *Numerical Recipes: The Art of Scientific Computing*, 3rd ed., Cambridge Univ. Press, New York.
Proctor, D. (1981), VHF radio pictures of cloud flashes, *J. Geophys. Res.*, *86*(C5), 4041–4071, doi:10.1029/JC086iC05p04041.
Proctor, D. (1997), Lightning flashes with high origins, *J. Geophys. Res.*, *102*(D2), 1693–1706, doi:10.1029/96JD02635.
Rakov, V. A. (2008), Lightning electromagnetic environment: From continuing-current fields to X-rays, in *Intl. Conf. on Grounding and Earthing & 3rd Intl. Conf. on Lightning Phys. and Effects*, Florianopolis, Brazil.
Rakov, V. A. (2013), Electromagnetic methods of lightning detection, *Surv. Geophys.*, *34*(4), 731–753, doi:10.1007/s10712-013-9251-1.
Rakov, V. A., and M. A. Uman (2003), *Lightning: Physics and Effects*, Cambridge Univ. Press, New York.
Romero, C., M. Paolone, F. Rachidi, M. Rubinstein, A. Rubinstein, G. Diendorfer, W. Schulz, M. Bernardi, and C. A. Nucci (2011), Preliminary comparison of data from the säntis tower and the euclid lightning location system, *XIth International Symposium on Lightning Protection* (*SIPDA*), Fortaleza, Brazil, 3–7 Oct.
Rubinstein, M. (1995), On the determination of the flash detection efficiency of lightning location systems given their stroke detection efficiency, in *11th Intl. Zurich Symposium on Electromagnetic Compatibility*.
Rubinstein, M., and E. Montandon (1992), Estimation of the stroke detection efficiency of two adjacent lightning positioning systems in Europe, in *22nd International Conference on Lightning Protection*, paper R 1b-05, Berlin.
Rudlosky, S. D. (2014), Evaluating ground-based lightning detection networks using TRMM/LIS observations, in *23rd International Lightning Detection Conference & 5th International Lightning Meteorology Conference*, Vaisala Inc., Tucson, Ariz.
Rudlosky, S. D., and D. T. Shea (2013), Evaluating WWLLN performance relative to TRMM/LIS, *Geophys. Res. Lett.*, *40*, 2344–2348, doi:10.1002/grl.50428.
Said, R., U. Inan, and K. Cummins (2010), Long-range lightning geolocation using a VLF radio atmospheric waveform bank, *J. Geophys. Res.*, *115*, D23108, doi:10.1029/2010JD013863.
Said, R., M. Cohen, and U. Inan (2013), Highly intense lightning over the oceans: Estimated peak currents from global GLD360 observations, *J. Geophys. Res.*, *118*, 6905–6915, doi:10.1002/jgrd.50508.
Schulz, W. (1997), Performance evaluation of lightning location systems, PhD thesis, Technical Univ. of Vienna, Vienna.
Schulz, W., and K. L. Cummins (2008), A method to determine relative stroke detection efficiencies from multiplicity distributions, in *20th International Lightning Detection Conference & 2nd International Lightning Meteorology Conference*, Tucson, Ariz.
Schulz, W., C. Vergeiner, H. Pichler, G. Diendorfer, and S. Packet (2012), Validation of the Austrian Lightning Location System ALDIS for negative flashes, in *Proc. CIGRE Symposium*.
Schulz, W., H. Pichler, G. Diendorfer, C. Vergeiner, and S. Pack (2013), Validation of detection of positive flashes by the Austrian Lightning Location System (ALDIS), in *12th Intl. Symposium on Lightning Protection (XII SIPDA)*, paper 2.2, Belo Horizonte, Brazil.
Schulz, W., S. Pedeboy, C. Vergeiner, E. Defer, and W. Rison (2014), Validation of the EUCLID LLS during HyMeX SOP1, in *23rd International Lightning Detection Conference & 5th International Lightning Meteorology Conference*, Vaisala Inc., Tucson, Ariz.
Serhan, G., M. Uman, D. Childers, and Y. Lin (1980), The RF spectra of first and subsequent lightning return strokes in the 1-to 200-km range, *Radio Sci.*, *15*(6), 1089–1094, doi:10.1029/RS015i006p01089.
Shao, X., and P. Krehbiel (1996), The spatial and temporal development of intracloud lightning, *J. Geophys. Res.*, *101*(D21), 26,641–26,668, doi:10.1029/96JD01803.
Shindo, T., et al. (2012), Lightning occurrence characteristics in Japan for 17 years: Observation results with lightning location systems of electric power utilities from 1992 to 2008, *IEEJ Trans. Electr. Electr. Eng.*, *7*(3), 251–257.
Sparrow, J., and E. Ney (1971), Lightning observations by satellite, *Nature*, *232*, 540–541.
Stock, M. G., M. Akita, P. R. Krehbiel, W. Rison, H. E. Edens, Z. Kawasaki, and M. A. Stanley (2014), Continuous broadband digital interferometry of lightning using a generalized cross-correlation algorithm, *J. Geophys. Res. Atmos.*, *119*, 3134–3165, doi:10.1002/2013JD020217.

Sugita, A., and M. Matsui (2012), Lightning characteristics in Japan observed by the JLDN from 2000 to 2010, in *22nd International Lightning Detection Conference & 4th International Lightning Meteorology Conference*, Broomfield, Colo.

Sun, Z., X. Qie, M. Liu, D. Cao, and D. Wang (2013), Lightning VHF radiation location system based on short-baseline TDOA technique—Validation in rocket-triggered lightning, *Atmos. Res.*, *129*, 58–66.

Suszcynsky, D., A. Jacobson, J. Fitzgerald, C. Rhodes, E. Tech, and D. Roussel-Dupre (2000), Satellite-based global lightning and severe storm monitoring using VHF receivers, in *16th International Lightning Detection Conference*, Tucson, Ariz.

Suszcynsky, D. M., T. E. Light, S. Davis, J. L. Green, and J. L. L. Guillen (2001), Coordinated observations of optical lightning from space using the FORTE photodiode detector and CCD imager, *J. Geophys. Res.*, *106*(D16), 17,897–17,906, doi:10.1029/2001JD900199.

Thomas, R., P. Krehbiel, W. Rison, T. Hamlin, D. Boccippio, S. Goodman, and H. Christian (2000), Comparison of ground-based 3-dimensional lightning mapping observations with satellite-based LIS observations in Oklahoma, *Geophys. Res. Lett.*, *27*(12), 1703–1706, doi:10.1029/1999GL010845.

Thomas, R., P. Krehbiel, W. Rison, T. Hamlin, J. Harlin, and D. Shown (2001), Observations of VHF source powers radiated by lightning, *Geophys. Res. Lett.*, *28*(1), 143–146, doi:10.1029/2000GL011464.

Thomas, R. J., P. R. Krehbiel, W. Rison, S. J. Hunyady, W. P. Winn, T. Hamlin, and J. Harlin (2004), Accuracy of the Lightning Mapping Array, *J. Geophys. Res.*, *109*, D14207, doi:10.1029/2004JD004549.

Thompson, K., M. Bateman, and L. Carey (2014), A comparison of two ground-based lightning detection networks against the satellite-based Lightning Imaging Sensor (LIS), *J. Atmos. Oceanic Technol.*, *31*, 2191–2205, doi:10.1175/JTECH-D-13-00186.1.

Thomson, E. M., M. A. Galib, M. A. Uman, W. H. Beasley, and M. J. Master (1984), Some features of stroke occurrence in Florida lightning flashes, *J. Geophys. Res.*, *89*(D3), 4910–4916, doi:10.1029/JD089iD03p04910.

Turman, B. (1978), Analysis of lightning data from the DMSP satellite, *J. Geophys. Res.*, *83*(C10), 5019–5024, doi:10.1029/JC083iC10p05019.

Turman, B., and R. Tettelbach (1980), Synoptic-scale satellite lightning observations in conjunction with tornadoes, *Mon. Weather Rev.*, *108*(11), 1878–1882.

Ushio, T., T. Wu, and S. Yoshida (2015), Review of recent progress in lightning and thunderstorm detection techniques in Asia, *Atmos. Res.*, *154*, 89–102, doi:10.1016/j.atmosres.2014.10.001.

Vonnegut, B., O. H. Vaughan, and M. Brook (1983), Photographs of lightning from the space shuttle, *Bull. Am. Meteorol. Soc.*, *64*, 150–151.

Vorpahl, J., J. Sparrow, and E. Ney (1970), Satellite observations of lightning, *Science*, *169*(3948), 860–862.

Warner, T. A., K. L. Cummins, and R. E. Orville (2012), Upward lightning observations from towers in Rapid City, South Dakota and comparison with National Lightning Detection Network data, 2004–2010, *J. Geophys. Res.*, *117*, D19109, doi:10.1029/2012JD018346.

Watson, A., R. Holle, and R. Lopez (1995), Lightning from two national detection networks related to vertically integrated liquid and echo-top information from WSR-88D radar, *Weather Forecasting*, *10*(3), 592–605.

Weidman, C., E. Krider, and M. Uman (1981), Lightning amplitude spectra in the interval from 100 kHz to 20 MHz, *Geophys. Res. Lett.*, *8*(8), 931–934. doi:10.1029/GL008i008p00931.

Willett, J. C., J. C. Bailey, V. P. Idone, A. Eybert-Berard, and L. Barret (1989a), Submicrosecond intercomparison of radiation fields and currents in triggered lightning return strokes based on the transmission-line model, *J. Geophys. Res.*, *94*(D11), 13,275–13,286, doi:10.1029/JD094iD11p13275.

Willett, J. C., J. C. Bailey, and E. P. Krider (1989b), A class of unusual lightning electric field waveforms with very strong high-frequency radiation, *J. Geophys. Res.*, *94*(D13), 16,255–16,267, doi:10.1029/JD094iD13p16255.

Zhang, D., K. L. Cummins, and A. Nag (2015), Assessment of cloud lightning detection by the U.S. National Lightning Detection Network using video and Lightning Mapping Array observations, in *Seventh Conference on the Meteorological Applications of Lightning Data*, Am. Meteorol. Soc., Phoenix, 4–8 Jan.